79-76T

①

LEVEL II

AD A065475

DDC FILE COPY

THESIS

MEASUREMENT OF THUNDERSTORM CLOUD-TOP PARAMETERS USING HIGH-FREQUENCY SATELLITE IMAGERY

Submitted by

Stephen Paul Pryor

Atmospheric Science Department

In partial fulfillment of the requirements
for the Degree of Master of Science
Colorado State University
Fort Collins, Colorado
Summer, 1978

79 02 26 235

UNCLASSIFIED
SECURITY CLASSIFICATION OF THIS PAGE (When Data Entered)

REPORT DOCUMENTATION PAGE	READ INSTRUCTIONS BEFORE COMPLETING FORM
1. REPORT NUMBER (19) CI-79-76T (18) AFIT	2. GOVT ACCESSION NO.
	3. RECIPIENT'S CATALOG NUMBER
4. TITLE (and Subtitle) (6) Measurement of Thunderstorms Cloud-Top Parameters Using High-Frequency Satellite Imagery	5. TYPE OF REPORT & PERIOD COVERED Thesis
	6. PERFORMING ORG. REPORT NUMBER
7. AUTHOR(s) (10) Stephen Paul Pryor	8. CONTRACT OR GRANT NUMBER(s) 9 Mast[illegible]
9. PERFORMING ORGANIZATION NAME AND ADDRESS AFIT student at Colorado State University	10. PROGRAM ELEMENT, PROJECT, TASK AREA & WORK UNIT NUMBERS (11)
11. CONTROLLING OFFICE NAME AND ADDRESS AFIT/CI WPAFB OH 45433 (12) 111p.	12. REPORT DATE Summer 1978
	13. NUMBER OF PAGES 101
14. MONITORING AGENCY NAME & ADDRESS (if different from Controlling Office)	15. SECURITY CLASS. (of this report) UNCLASSIFIED
	15a. DECLASSIFICATION/DOWNGRADING SCHEDULE

16. DISTRIBUTION STATEMENT (of this Report)

Approved for Public Release, Distribution Unlimited

17. DISTRIBUTION STATEMENT (of the abstract entered in Block 20, if different from Report)

18. SUPPLEMENTARY NOTES

1979

JOSEPH P. HIPPS, Major, USAF
Director of Information, AFIT

ORIGINAL CONTAINS COLOR PLATES: ALL DDC REPRODUCTIONS WILL BE IN BLACK AND WHITE

19. KEY WORDS (Continue on reverse side if necessary and identify by block number)

20. ABSTRACT (Continue on reverse side if necessary and identify by block number)

088 310

DD FORM 1 JAN 73 1473 EDITION OF 1 NOV 65 IS OBSOLETE

UNCLASSIFIED
SECURITY CLASSIFICATION OF THIS PAGE (When Data Entered)

COLORADO STATE UNIVERSITY

Summer 1978

WE HEREBY RECOMMEND THAT THE THESIS PREPARED UNDER OUR SUPERVISION

BY Stephen Paul Pryor

ENTITLED Measurement of Thunderstorm Cloud-Top Parameters Using High-Frequency Satellite Imagery

BE ACCEPTED AS FULFILLING IN PART REQUIREMENTS FOR THE DEGREE OF

Master of Science

Committee on Graduate Work

William R. Cotton

Thomas H Vonder Haar

Adviser

77-765

ABSTRACT OF THESIS

MEASUREMENT OF THUNDERSTORM CLOUD-TOP PARAMETERS USING HIGH-FREQUENCY SATELLITE IMAGERY

Variations of thunderstorm cloud-top parameters are examined using high temporal frequency satellite digital data. The day chosen as a case study, 5 May 1977, featured an extensive severe weather outbreak and was part of the Research Rapid Scan Day program during which three-minute interval satellite data was collected from GOES-1.

Overshooting top heights, measured by a shadow casting method, are added to infrared-determined heights and compared to radar echo top heights. Good agreement is noted between satellite-determined tops and radar echo tops. Overshooting tops are significantly higher just prior to hail occurrences than for tornado occurrences. Infrared imagery is found not to be adequate to reliably identify overshooting tops. Growth rate diagrams for five storms yield little in the way of signatures which would be an aid in prediction of severe weather events. An image differencing technique is demonstrated which may be of some aid in quantitatively measuring thunderstorm growth and advection.

This study stresses the analysis of digital satellite data with a sophisticated video imaging system, the All Digital Video Imaging System for Atmospheric Research (ADVISAR) at Colorado State University.

Stephen Paul Pryor
Atmospheric Science Department
Colorado State University
Fort Collins, Colorado 80523
Summer, 1978

ACKNOWLEDGEMENTS

For their assistance in preparing this paper, I wish to thank my committee members, Dr. Thomas H. Vonder Haar, Dr. William R. Cotton, and Dr. Daryl B. Simons. A critical review of the manuscript and technical assistance were provided by David W. Reynolds. Special thanks go to the Atmospheric Sciences Laboratory Direct Readout Ground Station (DRGS) at White Sands Missile Range (WSMR) for recording the satellite data and providing facilities for sectorizing and digitizing the data.

Other help at Colorado State University included drafting of figures by Mark Howes, photographic services by Mr. Duane Barnhart, and typing of the manuscript by Ms. Karen Greiner. This research was supported by National Science Foundation (NSF) Grant no. ATM76-21307.

TABLE OF CONTENTS

LIST OF TABLES

LIST OF FIGURES

Figure

Figure

1.0 INTRODUCTION

With the advent of the Applications Technology Satellites (ATS) in the late 60's meteorologists were given an essentially stationary platform from which to study the earth's weather. For the first time relatively short-time interval images could be obtained to observe cloud motion, growth, and development. Even though the ATS series observed the earth only in the visible, it was possible to gain new insights into the behavior of weather systems, both on the synoptic scale and mesoscale. Improved resolution visible imagery (.9 km) and the introduction of an infrared (IR) sensor on the Synchronous Meteorological and Geostationary Operational Environmental Satellites (SMS/GOES) have further expanded the possibilities for observation of small-scale variations in clouds and cloud systems. It is now possible to examine individual thunderstorm cells and closely monitor their behavior in the hope of detecting clues that will indicate which cells will produce severe weather and a potential threat to life and property.

This paper features the use of the highest time frequency satellite data yet available, the three-minute interval data recorded by GOES-1 as a part of the Research Rapid Scan Day (RRSD) Plan for 1977. These data are processed and analyzed with the aid of the All Digital Video Imaging System for Atmospheric Research (ADVISAR). This system is a sophisticated image display and analysis system developed by atmospheric scientists and engineers at Colorado State University for the analysis of digital satellite and similar data sets.

With the availability of such high frequency information it is possible to examine convective activity in great detail. This paper examines short-term variations in thunderstorm cloud tops and attempts to correlate the variations with severe weather occurrences. Several different techniques are presented that appear to be useful in examining cloud-top variations.

The day chosen as a case study for this paper is 5 May 1977. On this day an extensive severe weather outbreak occurred in an area from Texas to Illinois. Numerous occurrences of tornadoes and hail were reported. It was one of eleven days chosen for special satellite scanning as a part of the RRSD program, so an excellent satellite data set is available for study.

Protrusions through the cirrus anvil of a thunderstorm are indicative of the strength of the updrafts in the storm. These protrusions are referred to as overshooting tops. Several attempts have been made to study overshooting tops from aircraft (Lee, 1971; Fujita, 1974; Shenk, 1974; Pearl, 1975; Umenhofer, 1975). Only Fujita (1972) attempted to measure overshooting top heights from satellite imagery. A common method of measuring convective cloud-top heights is to use the IR black body temperature at cloud top assuming it is the same as the environmental temperature measured by radiosonde. It has been shown that this measurement greatly underpredicts the height when compared to the corresponding radar echo top (Negri, 1977). This is caused by the poor resolution of the IR sensor (∿ 8 km). The IR sensor simply does not "see" the overshooting top. Using the visible channel of GOES, overshooting top heights can be measured provided the top is casting a shadow on the cirrus anvil. Short-term variations of the top heights can then be examined in relation to weather events at the surface. With the availability of both visible and infrared sensors it is possible to combine measurements from the two channels to obtain a cloud-top height estimate referenced to mean sea level. These heights may be compared to radar echo heights to estimate their accuracy.

The infrared channel of GOES provides information on the cloud-top temperature of thunderstorm cells. By monitoring the variations in the minimum cloud-top temperature it is possible to gain information on the relative severity of the storm (Adler and Fenn, 1976, 1977). Such monitoring is easily accomplished which makes it applicable for operational use.

Another method of monitoring thunderstorm cloud-top variations in the IR is to monitor the expansion within certain cloud-top isotherms. The rate of expansion of such areas can be related to cloud-top divergence and thus gives some indication of the intensity of updrafts in the cloud. The variations in the size of these areas can be compared to severe weather occurrences in order to detect any relationship.

The differencing of two images obtained at different scan times produces a resultant image which contains information on the change between the two images. Such information can easily be quantified using the ADVISAR. This provides an easily obtainable measure of cloud growth, development and advection.

The advantage of developing satellite techniques to observe cloud-top variations in relation to severe weather occurrences can easily be seen. An entire area of potential and active severe weather can be monitored at one location thus reducing time and space problems inherent in other observing systems. One drawback to satellite observations is that the digital data needed for any quantitative measurements require computer processing to be useful. It is hoped, however, that high frequency satellite imagery can make a contribution to severe storm prediction and detection.

2.0 CASE STUDY: 5 May 1977

2.1 Synoptic Situation

The sequence of weather events leading to the formation of severe weather on 5 May 1977 can be traced back several days. On 2 May a very weak zonal flow at 500 mb existed across the central portion of the United States. An intense low pressure area in the Gulf of Alaska was moving to the east causing troughing along the west coast. Another short wave was present well to the south of this system approximately 2000 km west of Baja California. Two distinct flow patterns were present, one across the northwestern U.S., the other into the southwestern U.S. This pattern continued during the next 48 hours as a vigorous short wave moved into the western U.S. on 4 May. As this system moved into the Great Plains encountering warm, humid, tropical air, severe weather was touched off on the 4th. Tornadoes, hail, and high winds were reported in Kansas, Iowa, and Missouri causing considerable property damage and injuries.

By morning on 5 May conditions were developing for another severe weather outbreak. Figure 2-1 shows the 500 mb flow at 1200 GMT on 5 May. The intense low over the Pacific Northwest was now digging to the south. The weak short wave to the south had moved into the Southwest over southern New Mexico. Figure 2-2 shows the surface analysis of the south central U.S. at 1800 GMT on 5 May. The frontal system that moved across the Great Plains the previous day had become stationary from western Texas, across Kansas and Missouri into Illinois. The southern end of this stationary frontal system was beginning to show motion in response to the approach of the short wave in the Southwest. Tropical air with surface dewpoints generally above 65°F was present well into Kansas, Missouri, and Illinois extending into western Texas.

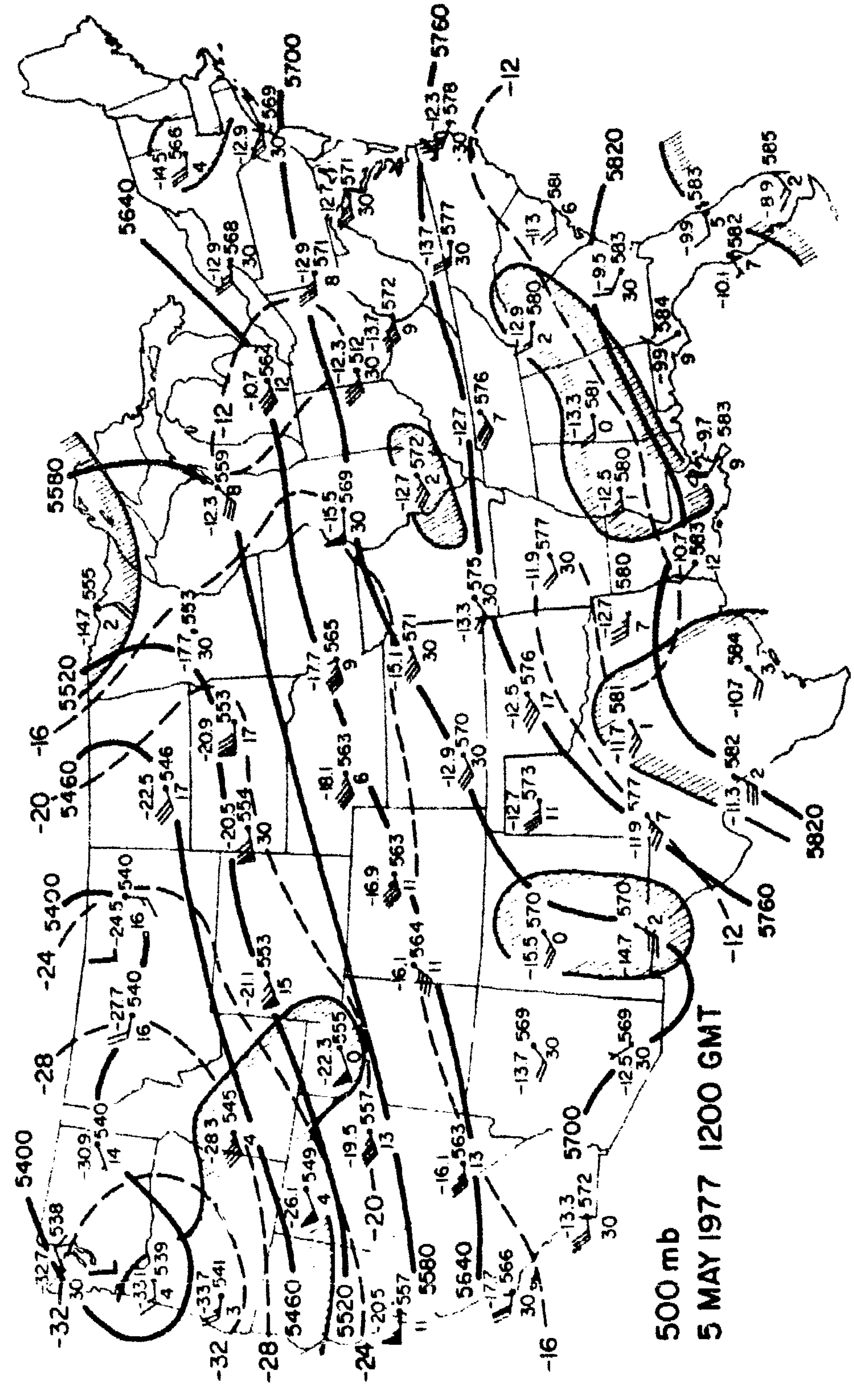

Figure 2-1 500 millibar analysis 5 May 1977 1200 GMT.

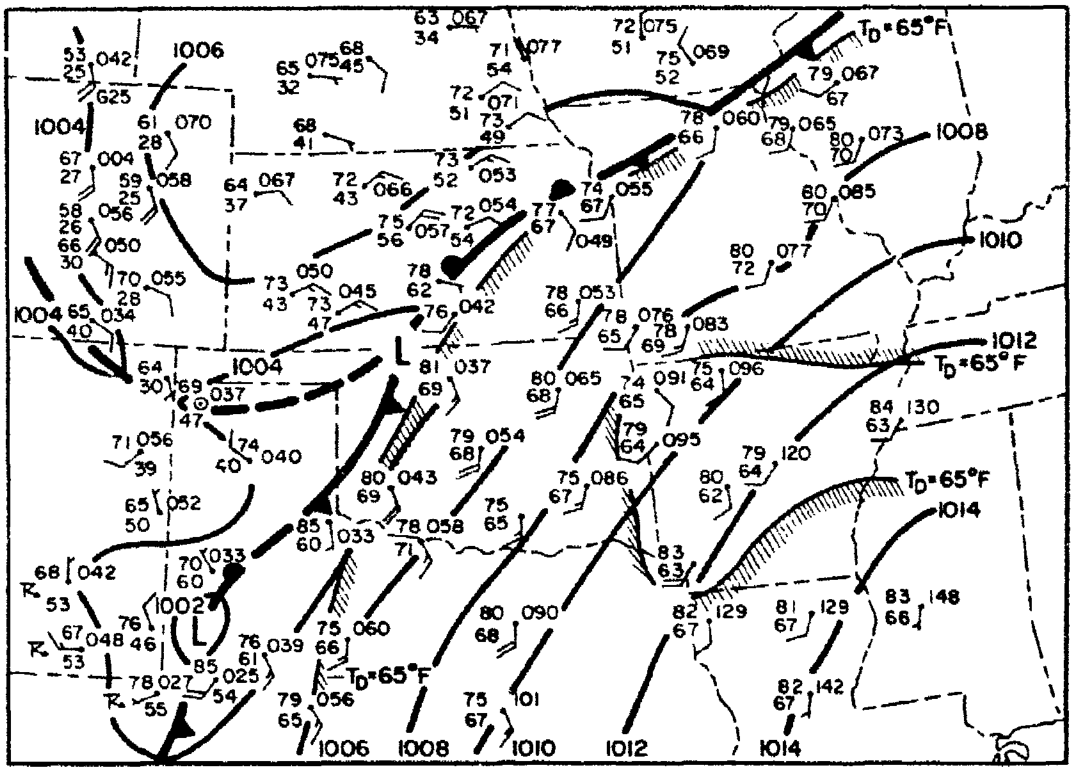

Figure 2-2 Surface analysis 5 May 1977 1800 GMT.

Figure 2-3 shows an analysis of the Total Totals stability index (Miller, 1972) and the Lifted index (Galway, 1956) for the south central U.S. at 1200 GMT. A Total Totals of 55 or greater and a Lifted index of -6 or less are considered to be strong indicators of potential severe thunderstorm activity (Miller, 1972). Based on values of these two stability indices, the maximum instability existed from eastern Kansas and northern Missouri to southern Iowa and eastern Illinois with the most unstable air in the vicinity of Topeka, Kansas. The large gradient in the Totals index to the west of Topeka is attributable to the presence of the stationary front shown in Figure 2-2. Figure 2-3 shows an area of maximum instability to the east and south of the surface front.

It is apparent that two separate mechanisms were operating to set off thunderstorm activity on 5 May. Western Texas, though not possessing the highest values of instability, was under the influence of a synoptic scale wave most easily discernable at 500 mb (Figure 2-1). This wave served to destabilize the atmosphere through cold air advection as well as providing large scale lifting. Additionally, the circulation at the surface was organized with the formation of a meso-low on the cold front near the Texas-New Mexico border (Figure 2-2). Areas to the northeast (Kansas, Missouri) were under no such synoptic scale forcing, but the values of instability were extremely large. In such conditions thunderstorms and severe weather can easily be produced by mesoscale phenomena.

2.2 Severe Weather Occurrences

On 5 May an extensive area of severe weather occurred mainly just to the south and east of the stationary front described in the previous section. Severe weather occurrences are plotted in Figure 2-4 in addition to severe weather watch areas forecast by the National Weather

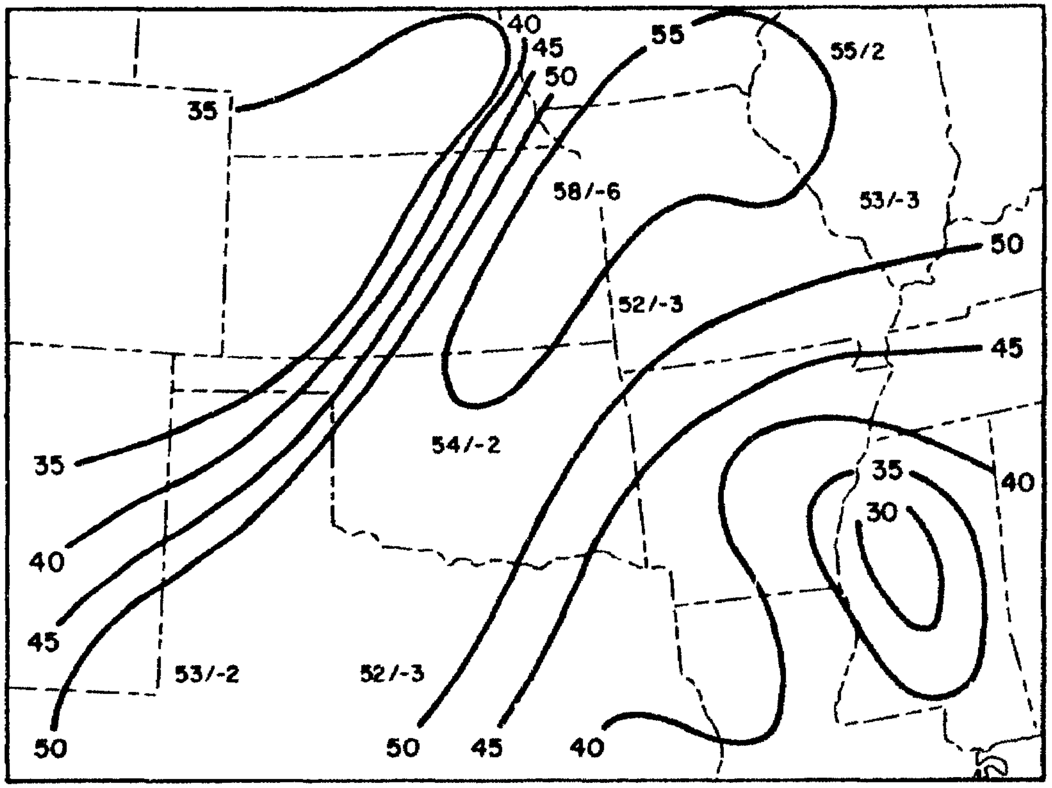

Figure 2-3 Analysis of Total Totals stability index 5 May 1977 1200 GMT. Values of the Lifted index are given for selected stations.

Service (NWS). Severe weather reports were obtained from the logs of the National Severe Storm Forecast Center in Kansas City and from Storm Data.* A complete listing of severe weather occurrences is given in Appendix A.

The first severe weather reports of the day came from west Texas when 4.4 cm (1.75 in.) hail was reported at Pecos, Texas at 1715 GMT. Thunderstorms in this area continued to develop and move eastward into Oklahoma during the day. Of the more notable reports in this area were 7.0 cm (2.75 in.) hail near Grassland, Texas at 2050 GMT and numerous but short-lived tornadoes in an area southeast of Lubbock, Texas. Little damage occurred and there were no casualties.

Later in the day two other areas of severe weather broke out. Shortly after 2100 GMT thunderstorms began to develop west of Kansas City near Topeka, Kansas. At 2220 GMT 4.4 cm (1.75 in.) hail was reported at Topeka. At 2345 GMT a tornado touched down south of Topeka causing little damage. Several other reports of severe weather occurred in the vicinity of Kansas City for the next few hours.

A third area of thunderstorm activity and associated severe weather developed in an area from the Missouri-Iowa border to just west of St. Louis around 2100 GMT. These fast-growing thunderstorms produced several reports of tornadoes and large hail. Hailstones of up to 7.0 cm (1.75 in.) in diameter were observed at Philadelphia, IL at 0035 GMT. A tornado touched down at Middletown, IA at 2245 GMT. Several people were injured in eastern Illinois due to lightning strikes and high winds.

---

*A monthly publication of the Environmental Data Service of the National Oceanographic and Atmospheric Administration.

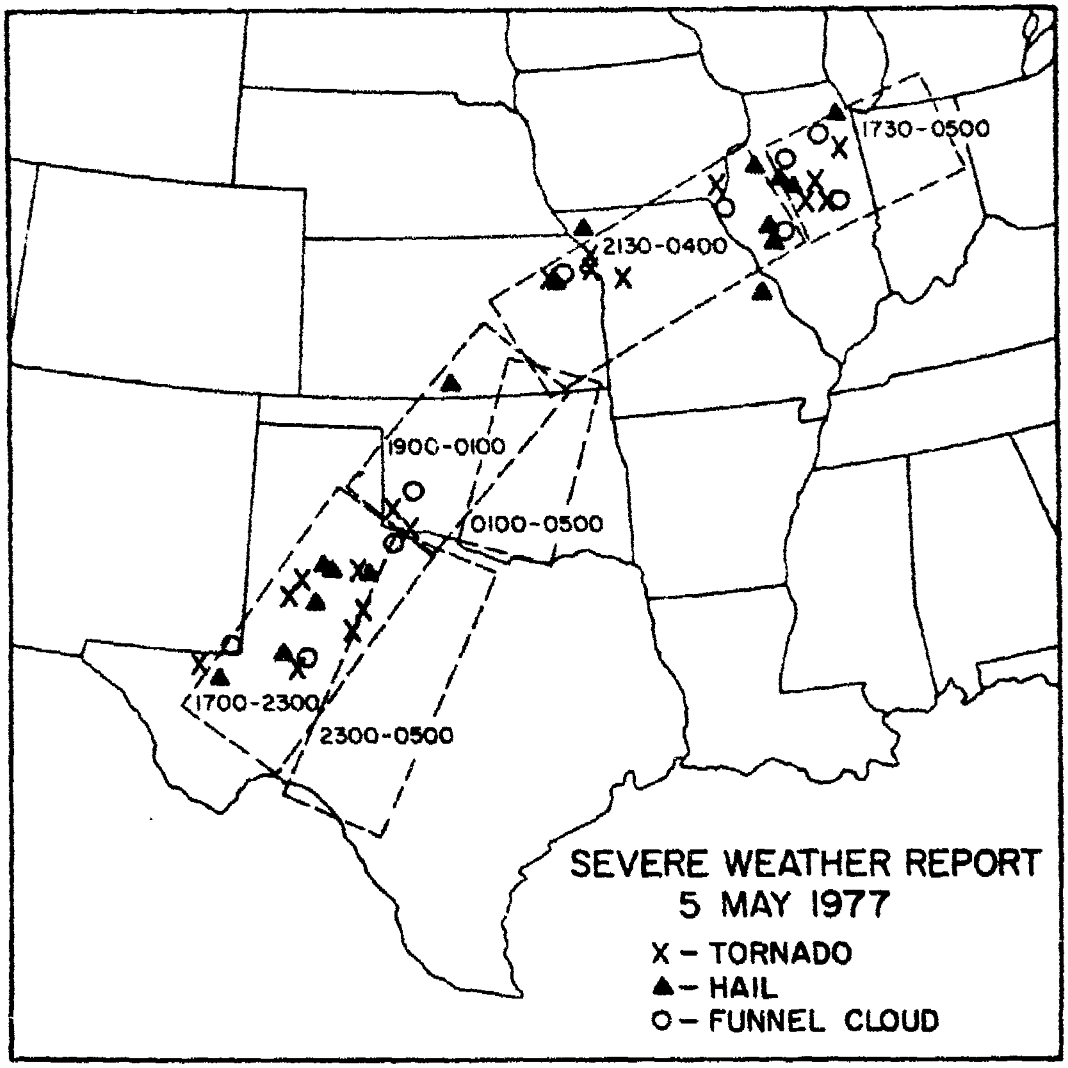

Figure 2-4 Severe weather occurrences and severe weather watch areas on 5 May 1977. Valid times for the watch areas are indicated in GMT.

There were no deaths due to weather in any of the above mentioned areas on 5 May.

3.0 DATA PROCESSING

3.1 Satellite Data

Digital satellite data for 5 May 1977 were obtained through the Direct Readout Ground Station (DRGS) at White Sands Missile Range, New Mexico (WSMR). The data were archived on magnetic tape at the ground station and were later sectorized and transferred to computer compatible digital tape for use on the All Digital Video Imaging System for Atmospheric Research (ADVISAR) at Colorado State University (CSU). A detailed explanation of the ADVISAR is given in Appendix B. Data received were from GOES-1 which on 5 May 1977 was in a geosynchronous orbit above the equator at approximately 75° west longitude. The sensing instrument was the Visible Infrared Spin-Scan Radiometer (VISSR) which contains eight visible channels operating in the 0.55 to 0.70 μm band and one infrared (IR) channel operating in the 10.5 to 12.6 μm band. The IR channel has a nominal subpoint resolution of 8 km (4.3 n.m.). The subpoint resolution in the visible channel is .9 km (.5 n.m.). The resolution deteriorates as the spot scanned by the satellite moves away from the subpoint. Visible resolution at 40°N, 90°W is approximately 1.3 km (.7 n.m.). The satellite scans the earth in a series of 1821 steps at 100 revolutions per minute. Further details of the GOES satellite and VISSR are given by McKowan (1975).

3.1.1 Research Rapid Scan Day

Satellite data for 5 May 1977 were obtained as part of the Research Rapid Scan Day (RRSD) program. This program was established to obtain 11, 8-hour periods of partial scan 3-minute data during the 1977 convective storm season. The RRSD Plan for 1977 stated that the reason for this short time interval data is "to provide the research community with data sets for studying tornadic storm formation, heavy convective rainfall, and convective processes in general".

Each data set was scheduled to run from 1700 GMT to 0100 GMT the following day. The schedule for an hour of data transmission is given in Table 3-1. As seen in the table the scans on the hour and half-hour consist of 800 scan lines. This allows the satellite to scan most of North America. The hour and half-hour scans are followed by six scans at three-minute intervals of 275 scan lines each. After the hour and half-hour scans and each three-minute scan the VISSR is retraced and set to start scanning at a point just north of the U.S.-Canadian border. However, this point is usually different for each image. So, the three-minute scans do not yield an image of exactly the same area on the earth although the same general region is scanned. At the beginning of the hour and half-hour scans the VISSR is retraced to the normal starting point used for a full earth scan, so spatial agreement among the day's hour and half-hour scans is almost exact.

The data for 5 May 1977 were sectorized and stored on digital tape in two parts. The IR data sector consisted of 250 scan lines extending from the Canadian-U.S. border to southern Texas and 600 elements extending generally from eastern Utah to near Chicago encompassing the central portion of the U.S. The visible data sector consisted of the same number of scan lines but the east-west dimension was the equivalent of only 500 IR (2000 visible) elements. However, the center points of the IR and visible sectors were identical for their respective image times. Approximate dimensions of the scanned areas with a view as seen by the satellite are illustrated in Figure 3-1.

Table 3-1 Schedule for Receipt of Data During RRSD (from RRSD Plan for 1977)

Time After Hour (Min:Sec)	Number of Scan Lines	Gridded
00:00	800	Yes
09:00	275	Yes
12:00	275	No
15:00	275	No
18:00	275	No
21:00	275	No
24:00	275	No
30:00	800	Yes
39:00	275	Yes
42:00	275	No
45:00	275	No
48:00	275	No
51:00	275	No
54:00	275	No

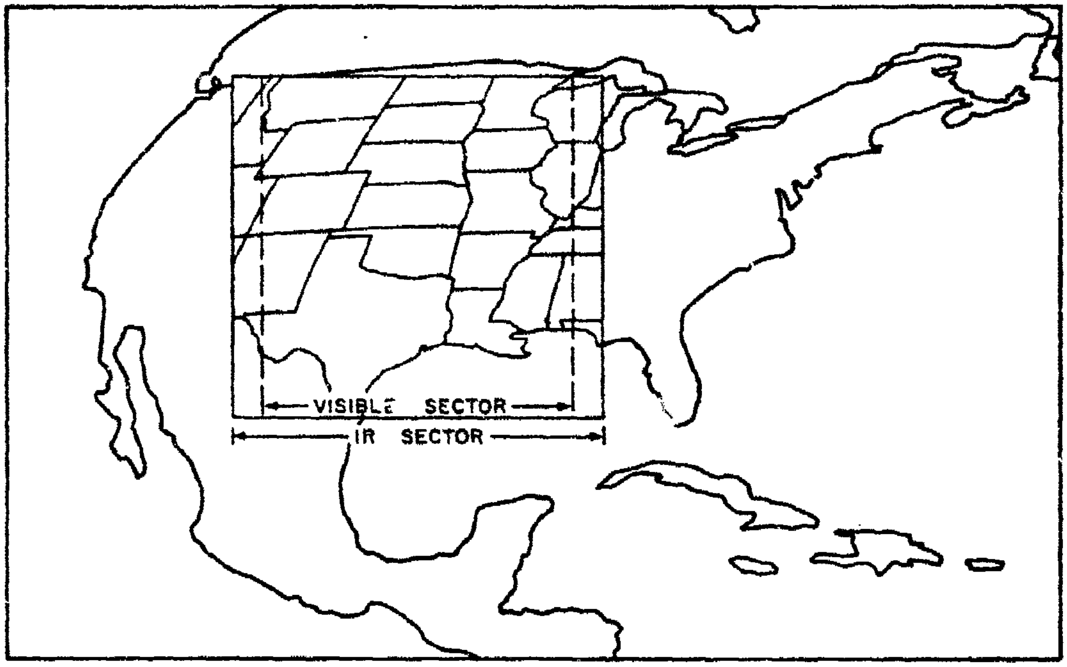

Figure 3-1 Infrared and visible sectors showing approximate areas scanned.

3.1.2 Image registration

Actual data obtained spans time periods from 1730 GMT to 0024 GMT for the IR data and from 1730 GMT to 0051 GMT for the visible. It was not possible to place the IR and visible data of the same imaging time on the same digital tape due to computer hardware and software problems at the DRGS. Similar problems also made it impossible to record line documentation. In the time periods given above, 98 IR images and 104 visible images were obtained and stored on tape for processing on the ADVISAR. Since the three-minute scans did not have the same start point for each image, it was necessary to manually register each image to a reference image by landmark matching. The IR data were processed in this manner first since they were available before the visible data. The landmark used initially was Oahe Reservoir located on the Missouri River in South Dakota. The registration was accomplished by storing the reference image and the image to be registered on two separate memory planes of the ADVISAR. Up to eight images can be stored. Then the image to be registered can be overlayed on the reference image and displayed on the video monitor. Adjustments can then be made to the lines and elements so that the two landmarks are perfectly overlayed. Any error in position will show up as a colored area on the monitor. The shift required in lines and elements is then recorded for future reference. After seven images are registered to the reference image the ADVISAR can be used to loop through the images in a repeating sequence. Any errors in registration show up as motion of the landmark. Further corrections can be made to remove any such motion. After 2321 GMT the reservoir became unusable as a landmark because the temperature difference between the land and water was such that the reservoir did not stand out from surrounding land areas in the IR. The western tip of Lake Superior was used to register the remaining images.

The visible data were registered in the same manner as the IR. The landmark used was Jackson Reservoir, a small lake approximately 2 km x 2 km in dimension located just east of Greeley, Colorado. After 2330 GMT decreasing brightness of the land surrounding the reservoir rendered it useless for any further registration. For the remaining images the Black Forest, a small forested area just east of Colorado Springs, was used. Due to the size of this area and the rapidly fading light, the remaining images were difficult to register. After 0030 GMT the procedure became impossible due to darkness. A list of the relative line and element shifts of each image, both in the IR and visible, is given in Appendix C.

3.1.3 Navigation

In order to interact with satellite data in a meaningful manner it is necessary to have some method of converting from a satellite reference frame (lines and elements) to an earth reference frame (latitude and longitude). This is essential for comparing earth located data such as radar, surface and upper air observations, and severe weather occurrences with satellite data. The process for this conversion from one reference frame to another is known as navigation.

The navigation algorithms used in this study are adaptations of those developed by Smith and Phillips (1972). This procedure uses orbital elements for the satellite to locate it in space at any given time. Orbital elements for 5 May 1977 for GOES-1 are given in Table 3-2. It is possible to locate any point on the earth in satellite coordinates by measuring the line and element position of a single reference

Table 3-2 Orbital Elements for GOES-1

Semi-major Axis	42167.265 km
Eccentricity	0.000224
Inclination	0.230°
Mean Anomaly	214.600°
Argument of Perigee	173.415°
Right Ascension of Ascending Node	115.536°
Right Ascension	218.543°
Declination	-89.856°
Epoch Time	77050100 GMT

landmark and by determining the latitude and longitude of the reference landmark and of the points to be located. The procedure can be reversed as well, converting points measured in satellite coordinates to latitude and longitude.

As a check on this procedure several known landmarks were located in satellite coordinates and then converted to latitude and longitude. The results of this check are given in Table 3-3. The reference landmark used was the center of a bend in the Mississippi River at Nauvoo, Illinois. In all cases the measurements are of a distinctive and easily recognizable feature. Position measurements in latitude and longitude were made using aeronautical navigation charts and could be determined to the nearest 30 seconds of latitude or longitude. The computer program used returns values to the nearest second. The average absolute latitudinal error was 1.1 km and the longitudinal error was 2.7 km. The size of a visible pixel in the north-south direction is approximately 1.3 km which is comparable to the error. In the east-west direction the pixel size is about 0.9 km which is about one-third the average error. It can be said with some confidence that the navigation was accurate to one pixel in the north-south direction and three pixels in the east-west direction. Some degree of error is inherent in the measurement processes both in earth and satellite coordinates but these errors would not account for the three pixel error in the east-west direction.

The navigation was accomplished only for the 1730 GMT image. Since the relative line and element displacements of the other images were determined by landmark registration, the navigation can be applied to all other images simply by adding the displacements to the navigated

Table 3-3 Navigation Check

Landmark	Navigated Position	Measured Position	Error (km)
De Gray Reservoir, AR	34°13'56"N	34°13'00"N	1.73
	93°08'54"W	93°08'00"N	2.91
Farmerville Reservoir, LA	32°44'53"N	32°44'30"N	.71
	92°25'14"W	92°24'00"W	1.92
Lake McConaughy, NE	41°18'26"N	41°18'00"N	.80
	102°04'02"W	102°05'00"W	-2.74
Harlan Reservoir, NE	40°04'39"N	40°04'00"N	1.20
	99°15'10"W	99°13'00"W	3.07

lines and elements from the reference image. Any known point in either satellite or earth coordinate system can be converted to the other system.

3.2 Supporting Data

More conventional data for this study were obtained from several sources. The Bureau of Reclamation made available hourly surface observations. Upper air data were obtained from the National Center for Atmospheric Research (NCAR). Radar data, including hourly radar summary charts, radar station observation logs, and Plan Position Indicator (PPI) films from selected stations, were obtained from the National Climatic Center in Asheville, NC.

4.0 DETERMINATION OF CONVECTIVE CLOUD HEIGHTS

The overshooting top of a thunderstorm cirrus anvil offers a potential source of information of the circulation within the storm. As a convective element rises through a storm, its rate of ascent depends on the temperature difference between it and the surrounding environmental air. As it passes through the tropopause, it becomes neutrally buoyant but still possesses a great deal of kinetic energy allowing it to penetrate the tropopause. Above the tropopause, the element is decelerated by negative buoyancy as it becomes colder than the stably stratified environment of the lower stratosphere. The degree of penetration, as indicated by an overshooting top, depends on the strength of the updraft velocity in the thunderstorm and the stability of the region in which the pentration is occurring.

Overshooting tops have been investigated for several years with a number of significant findings. Lee (1971) examined top protrusions using aircraft photography of storm tops. He concluded that the overshooting tops associated with tornado-producing storms were larger than those of other storms, but that such protrusions have an average height of only 0.6 km (2,000 feet). In a radar study of severe storms, Bonner and Kemper (1971) determined that above 10.7 km (35,000 feet) tornado probabilities are insensitive to echo top height. This says nothing about tops penetrating the cirrus anvil, however. Fujita (1972) measured top penetrations using ATS imagery and implied that tornadoes are most likely to occur when the overshooting top decreases in height. Shenk (1974), using aircraft observations, examined the variation of cloud top heights with time and determined an average maximum overshooting height of 1.6 km with horizontal dimensions of between 2.5 and 12.4 km suggesting only the larger tops could be resolved by the IR sensor of GOES. Pearl et.al. (1975) studied hail producing thunderstorms from aircraft and correlated the maximum height of the overshooting top with the onset of hail. Using aircraft photography, Fujita (1974) examined the period of oscillation of overshooting tops of various sizes and concluded that the height of a top or dome of diameter greater than 1.6 km (1 nm) is closely related to the intensity of the updrafts and downdrafts in the storm. Such large tops are readily detectable from GOES in the visible. Umenhofer (1975), studing tornado-producing thunderstorms, verified Fujita's hypothesis of a decrease in top height just prior to tornado occurrence.

In order to use such information in an operation manner, it is obvious that a geosynchronous satellite such as GOES is necessary. The high frequency data employed in this study is one possible method of examining overshooting tops.

4.1 Height Estimation Using Infrared Data

The determination of cloud-top heights through the use of GOES IR data is simple and straightforward lending itself to operational use. A few assumptions are necessary to use this method. First, the cloud emissivity is assumed to be equal to one so that the blackbody temperature of the cloud can be used to represent the actual cloud-top temperature. Cox (1977) determined that in cirrus outflow regions of thunderstorms, heights may be inferred to within 300 meters provided clouds are not below satellite resolution, so this seems to be a reasonable assumption. Second, the cloud-top temperature is assumed to equal that of the environment at the same height. Pitts et.al. (1975), using an aircraft instrumented with an infrared radiometer, determined that convective storm tops have an average temperature close to that of the environment. There were, however, anomalous hot and cold regions on horizontal scales of 50 to 1,000 m, well under the resolution of the GOES IR sensor.

The procedure of determining the top height involves simply taking the blackbody temperature of the cloud top and deriving the height from the nearest environmental sounding. Negri (1977) used this procedure and found that for cloud tops above the tropopause the IR-derived tops consistently underestimated the radar echo top. The reasons for this discrepancy as given by Negri are:

1) Lack of sufficient resolution in the IR sensor to detect small penetrations.
2) Finite response time of the IR sensor.
3) Entrainment of air above the tropopause which has a nearly isothermal lapse rate.

Theoretically a top penetrating the tropopause will continue to cool moist adiabatically. Thus, the lapse rate in the overshooting cloud will be moist adiabatic implying that the top should be much colder than its environment. In comparing the size of an IR pixel (37 km^2) to the size of typical overshooting tops (25 km^2), it is clear that the main problem is one of resolution. The coldest temperature at the top of the overshoot will occupy only a tiny fraction of the area of an IR pixel. Consequently, the IR sensor simply does not "see" the top.

4.2 Measurement of Overshooting Top Heights

An overshooting top can be seen penetrating the cirrus anvil when the sun elevation angle is low enough to permit a shadow to be cast on the anvil. Fujita (1972) used ATS visible imagery to determine the heights of overshooting tops by this method. Use of the improved resolution of GOES and the versatility of digital data allows for a more accurate determination of the top heights.

Fujita (1974) differentiates between an "overshooting dome" which has horizontal dimensions of between 1.8 and 18 km (1 to 10 miles) and an "overshooting turret" which has dimensions of less than 1 mile. Due to the resolution of the visible sensor (.9 km), the satellite can detect only the "overshooting domes" which will simply be referred to as "overshooting tops". A conceptual model of such an overshooting top is presented in Figure 4-1.

4.2.1 Method

To determine the height of the top above the cirrus anvil, two assumptions must be made:

1) The cirrus anvil on which the shadow is cast is relatively flat.
2) The point immediately beneath the top can be accurately determined.

As seen in Figure 4-1, the height can be calculated from the relation

$$h = d/\tan z \qquad (4\text{-}1)$$

where: z is the solar zenith angle

d is the distance from the center of the overshoot to the edge of the shadow.

The position of the sun in relation to any point on the earth must be known at any time. Particularly important are the solar zenith and azimuth angles. The geometry of the sun-earth relationship is illustrated in Figure 4-2. Sellers (1965) discussed these relationships in

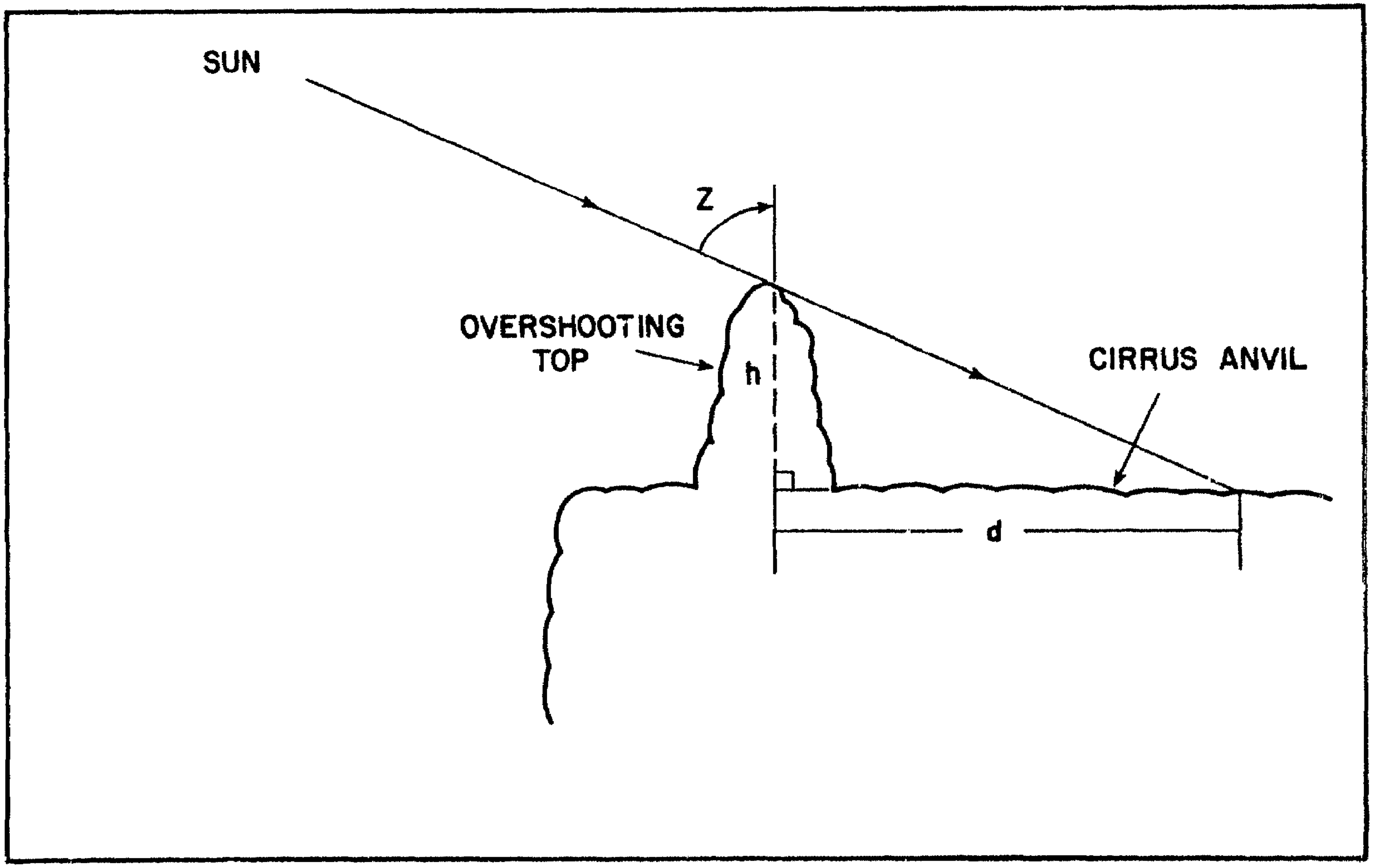

Figure 4-1 Conceptual model of an overshooting top.

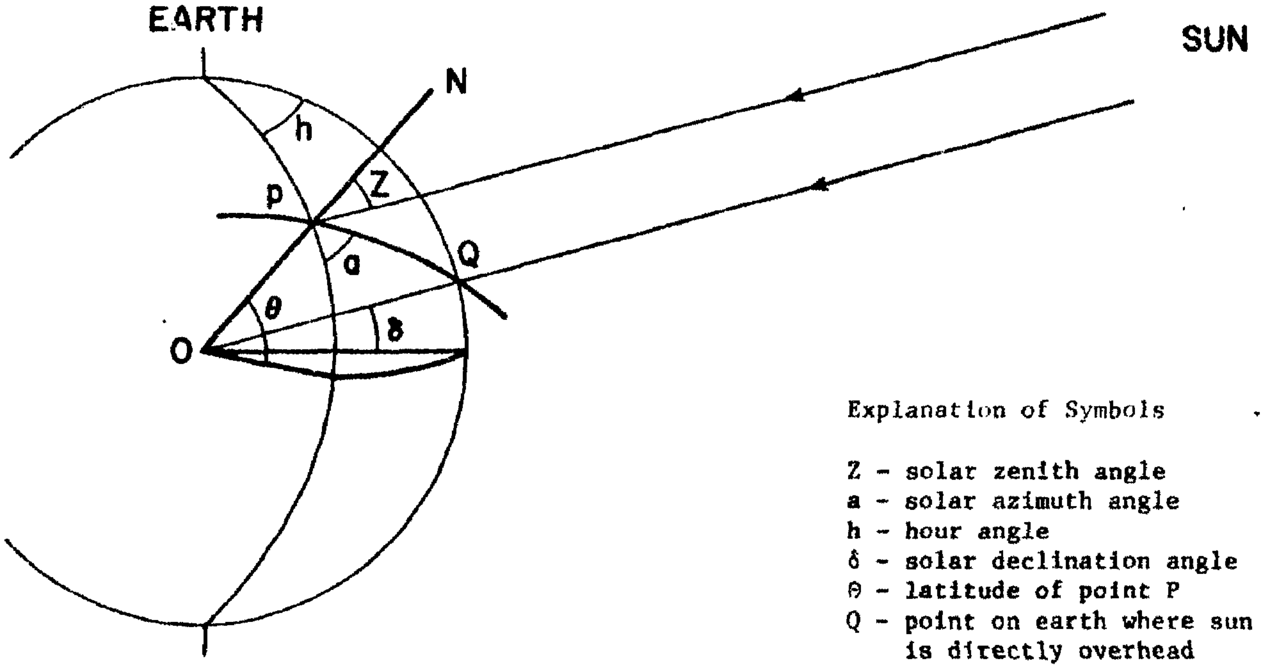

Explanation of Symbols

Z - solar zenith angle
a - solar azimuth angle
h - hour angle
δ - solar declination angle
θ - latitude of point P
Q - point on earth where sun is directly overhead

Figure 4-2 Geometry necessary to locate the sun in relation to point P.

some detail and presented the following equations for the zenith and azimuth angles:

$$\cos z = \sin \theta \sin \delta + \cos \theta \cos \delta \cos h \tag{4-2}$$

$$\cos a = \frac{\sin \theta \cos z - \sin \delta}{\cos \theta \sin z} \tag{4-3}$$

where θ is the latitude.

δ is the solar declination angle.

h is the hour angle.

z is the solar zenith angle.

a is the solar azimuth angle.

The azimuth angle must be known in order to determine the angle at which the sun intercepts the data.

The satellite-earth geometry must also be solved to determine the viewing angle of the satellite. Figure 4-3 illustrates this geometry. If point D is a point scanned at any moment, the vector $\vec{R}_e$ can be written locating $\dot{D}$ in terms of its components.

$$\vec{R}_e = R_e \left[\cos \theta \left(\hat{i} \cos \phi + \hat{j} \sin \phi\right) + \hat{k} \sin \theta\right] \tag{4-4}$$

where: R_e is the earth radius.

θ is the latitude of point D.

ϕ is the longitude of point D.

The earth-satellite vector $\vec{R}_s$ can similarly be expressed.

$$\vec{R}_s = R_s \left(\hat{i} \cos \phi_s + \hat{j} \sin \phi_s\right) \tag{4-5}$$

where: R_s is the distance from earth center to the satellite.

ϕ_s is the subpoint longitude.

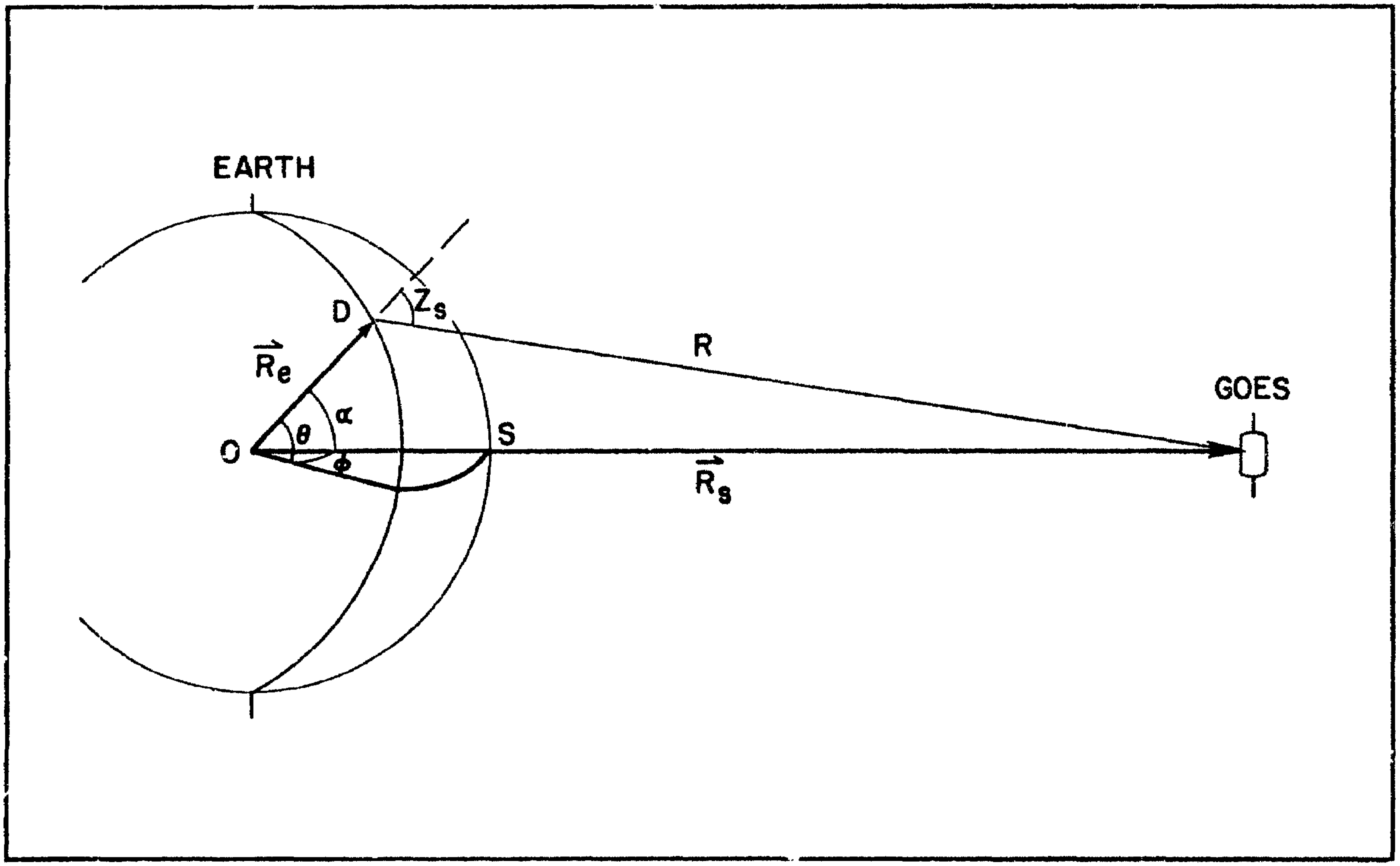

Figure 4-3 Satellite-Earth geometry.

Taking the vector dot product of R_s and R_e we can solve for α, the angle between the vectors.

$$\cos \alpha = \frac{\vec{R}_e \cdot \vec{R}_s}{R_e \quad R_s} \tag{4-6}$$

The satellite-earth distance R can be solved for through the law of cosines.

$$R^2 = R_e^{\ 2} + R_s^{\ 2} - 2R_s R_e \cos \alpha \tag{4-7}$$

Through the law of sines, the satellite zenith angle, z_s, can be determined.

$$\sin (\pi - z_s) = \frac{R_s \sin \alpha}{R} \tag{4-8}$$

Knowledge of z_s and α can be used to correct for error caused by the fact that the satellite is not scanning a spot on the earth but rather the top of a cirrus anvil 10 to 12 km above the earth. Figure 4-4 illustrates this relationship. The distance d_c necessary to locate the scan spot in true earth coordinates is given by

$$d_c = h \tan z_s \tag{4-9}$$

where: h is cloud height.

z_s is the satellite zenith angle.

In the area examined in this study tan $z_s \sim 1$ so that d_c is approximately equal to h. This distance ($\sim$ 15 km) is nearly an order of magnitude larger than the navigation error, thus the correction must be made.

The top height determination process begins by using the ADVISAR to display the data on the video monitor. Images in the visible and IR of the same image time are written onto two separate memory planes.

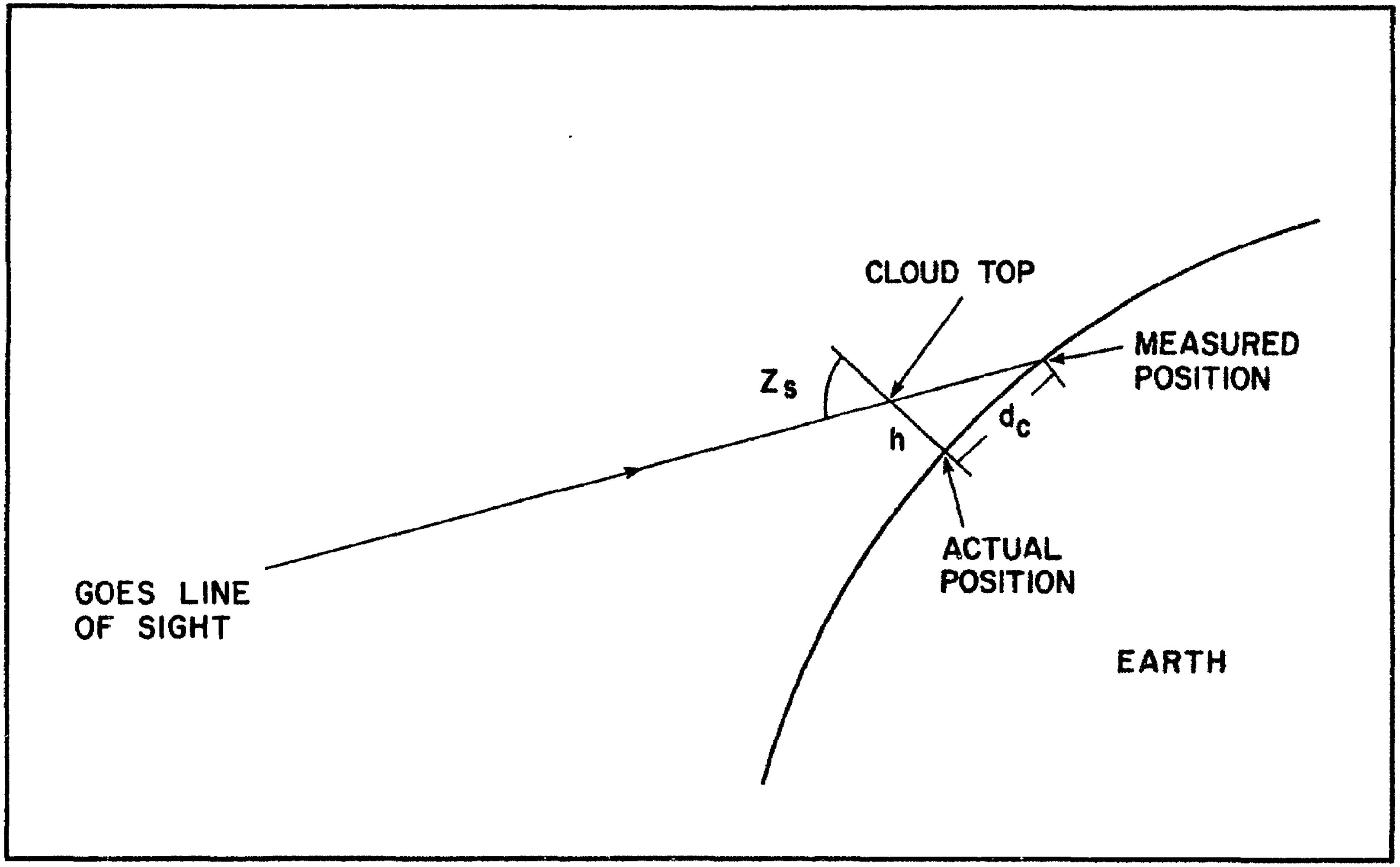

Figure 4-4 Depiction of error in location caused by satellite observation of cloud top.

The IR image is expanded to match the same area as displayed in the visible. An overshooting top is identified visually and surrounded with a box-like cursor. Data values in the visible and IR within the cursor are printed out. At the same time a threshold value for the shadow is determined. This value varies with the time of day. Through the navigation routines discussed in the previous chapter, the location of the top is determined in latitude and longitude. This location is corrected using a height obtained from the IR at the location of the overshoot. The solar azimuth and zenith angles are then computed. For the area considered in this study, the angle between a horizontal scan line of the satellite and a corresponding latitude circle is negligible. So for azimuth angles $\sim 90^{\circ}$ no additional correction need be made to the azimuth to obtain the angle the sun makes with the data array. From the visible data the number of pixels within the shadow along the two axes of the data grid are counted. With knowledge of pixel dimensions at a particular latitude and longitude, the length d (Figure 4-1) can be calculated which determines the height of the overshoot. Pixel dimensions, or rather the distance between the centers of adjacent scan spots, can be computed using the navigation routines.

As might be expected since h is proportional to cot z, the potential for error becomes very large at small zenith angles. Table 4-1 gives the error caused by a one pixel error in the measurement of a shadow along the scan direction of the satellite. This error is a measure of the vertical resolution. Since radar heights are given to the nearest 1,000 feet (.304 km), it would be desirable to make measurements at zenith angles that yield this amount of error. This angle is around 70°. Errors increase quite rapidly with zenith angles smaller than

Table 4-1

Error in Top Height Caused by a One Pixel Error in Length of a Shadow at 40°N, 90°W

Time (GMT)	Solar Zenith (Deg)	Error in Height (km)
2130	51.2	.671
2145	54.0	.606
2215	59.7	.487
2230	62.6	.432
2245	65.5	.380
2300	68.3	.331
2315	71.2	.284
2330	74.1	.238
2345	76.9	.194
0000	79.7	.151
0015	82.5	.110
0030	85.3	.069
0045	88.0	.029

this. In order to have reasonable confidence in the accuracy of the top calculations, no shadow measurements were made prior to 2215 GMT. A two pixel error will simply double the errors indicated in Table 4-1. Obviously the accurate determination of the shadow length is the most critical and important factor in the whole process.

A typical visible brightness pattern associated with an overshooting top and the corresponding IR data are illustrated in Figure 4-5 and Figure 4-6. Note the lack of variation in temperature in the IR image. The brightest area appears on the southwest side of the top due to the relative positions of the sun and satellite. The actual point representing the top is generally taken to be the first pixel from the shadow along the sun angle. However, some subjectivity must enter here since no two tops are alike. The shadow length is computed from this point.

4.2.2 Results

Over 100 cloud top protrusions were measured between 2215 GMT and 0024 GMT. No attempt was made to add the shadow height to the IR-determined height. This is done in the next section for comparison with radar. The sample included the entire area of convective activity for the day extending from Texas to Illinois. A plot of overshooting top heights versus solar zenith angle is given in Figure 4-7. Also plotted are curves for a one pixel error (1) and a two pixel error (2). These curves reveal that no tops were measured with a shadow length of less than two pixels. This represents a lower threshold of detection for overshooting tops. The scatter of points indicates that only the higher tops are measured at low zenith angles ($50-60^{\circ}$). This happens because small tops ($\sim$ 1 km) are below the detection threshold and

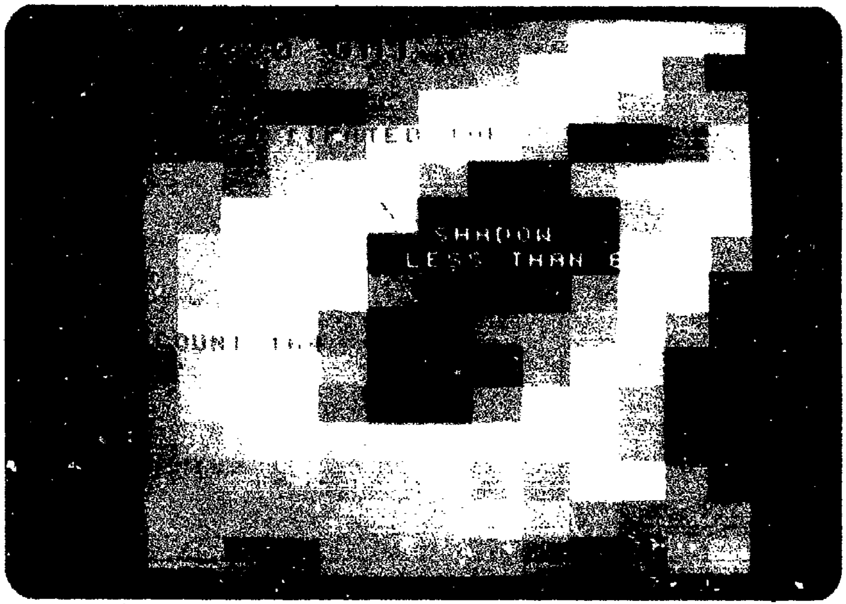

Figure 4-5 Visible brightness pattern of an overshooting top showing the individual pixels, blacked-out shadow, brightest pixel and estimated top.

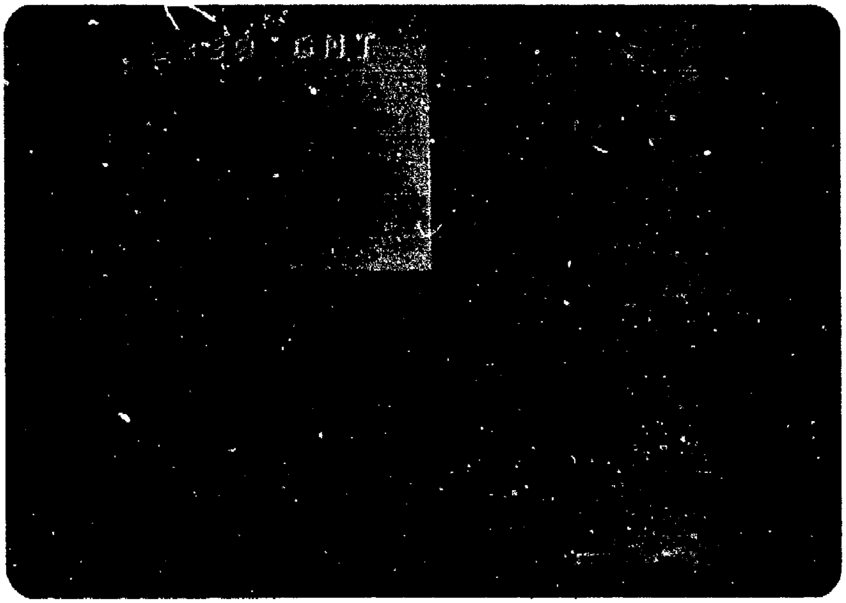

Figure 4-6 Collocated infrared image with temperature values displayed. Note lack of variation in temperature.

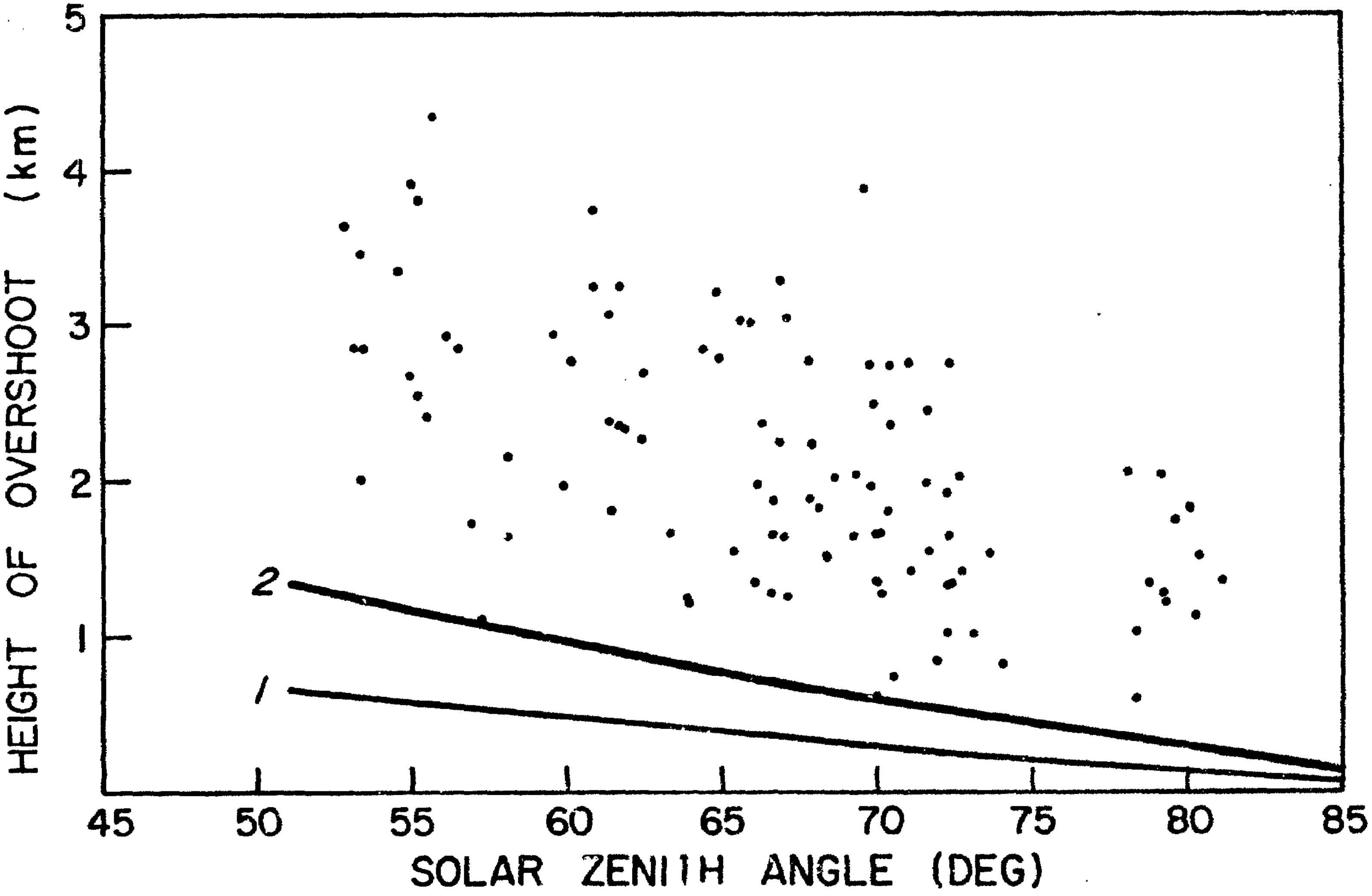

Figure 4-7 Measured overshooting [illegible] height versus solar zenith angle.

because a conscious effort was made to measure the larger tops. At large zenith angles ($\sim 80^{\circ}$) only small tops are measured. This is because the shadow length of large tops is too long to unambiguously measure. For the region between zenith angles of 60° and 75° there is a broad spectrum of measured values while the detection threshold has decreased below 1 km. These zenith angles represent about one and a half hours of time. It is felt that in this region the most accurate and consistent measurements are made.

4.3 Comparison of Visible and Infrared Top Heights

In order to test the accuracy of the two methods for determining the height of convective cloud tops, two imaging times were chosen which correspond with radar observation times. These were 2230 and 2330 GMT, times at which distinct shadows were being cast by overshooting tops. Since the IR sensor does not"see" these relatively small penetrations, the IR-derived temperatures should approximate the temperature of the cirrus anvil rather than that of the overshooting top. It should be possible therefore to combine the heights determined from the IR sensor and the heights of the overshoots determined from the shadow cast on the anvil top.

The calculated top heights were compared to radar echo heights at their respective times. Only those radar tops which could be closely correlated in position to a visible overshoot in the satellite data are presented. The results of this satellite-radar comparison are presented in Figure 4-8. The IR temperatures used to determine heights were not necessarily the same as those used to combine with the shadow heights. To simulate previous attempts at height measurement, the coldest

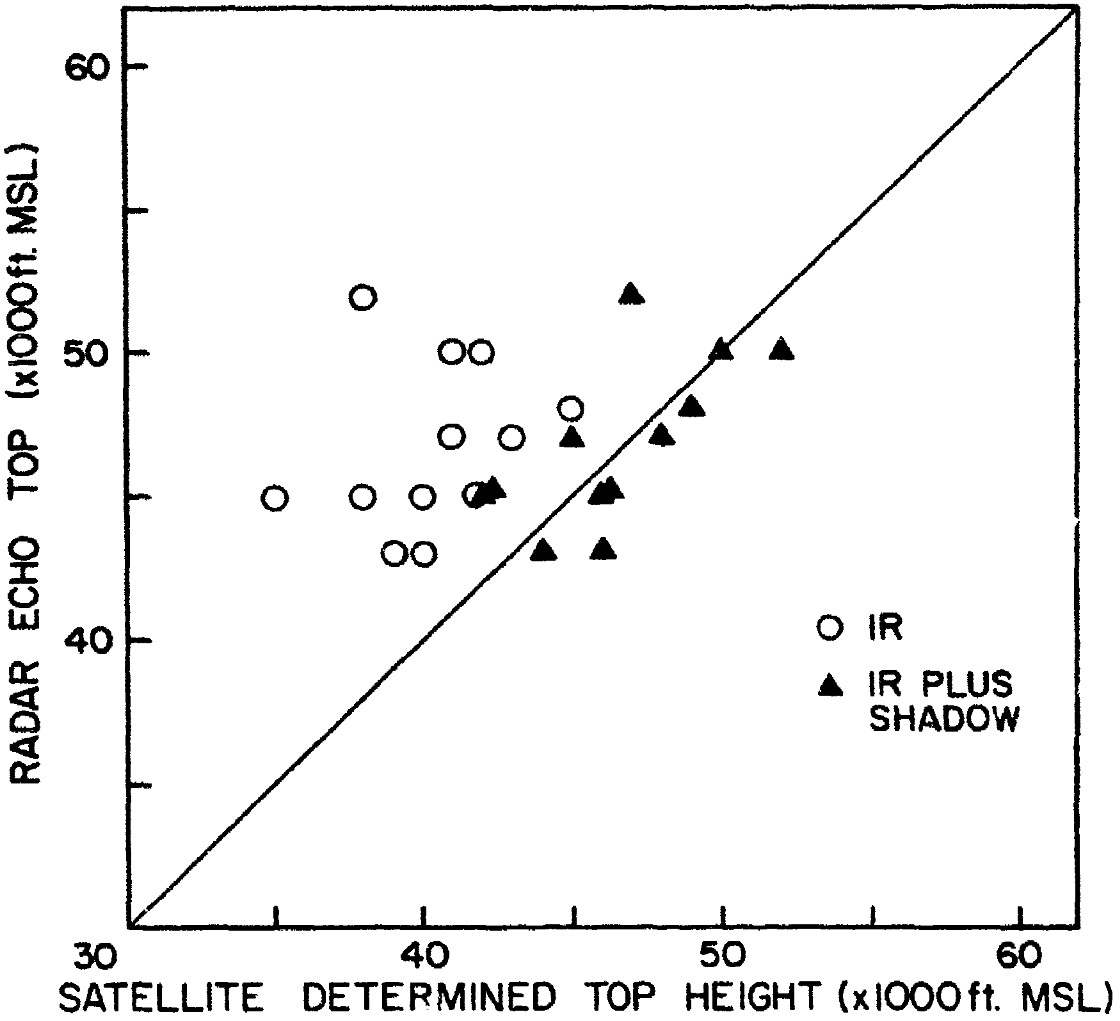

Figure 4-8 Comparison of radar echo top height and satellite determined cloud-top height.

temperature in the immediate vicinity of the overshoot was used to calculate the height. When calculating the shadow-determined heights, an attempt was made to use the temperature where the shadow was cast. No great amount of difference was noted, however.

Figure 4-8 clearly shows that the IR height determination method can be improved upon significantly by using the shadow method when applied to overshooting tops. The maximum difference in satellite and radar tops was 5,000 feet (1.52 km). All other tops were within 3,000 feet (.91 km) of the radar echo top. Using IR data only, measured tops were in error by as much as 14,000 feet (4.37 km) with no top closer than 3,000 feet (.91 km) to its radar-determined value.

It is well to note at this point that radar is detecting precipitation echoes while the visible channel of the VISSR is sensing the cloud. Saunders and Ronne (1962) compared visible tops and radar echoes at ranges of 10-35 nm and determined that actual cloud tops exceed radar echoes by 200 - 3,000 feet. However, radar echo top measurements tend to become less accurate with range. When observing intense storms, vertical distortions of actual echo tops increase with range. Donaldson (1964) discusses this problem in detail. Speed (1965) indicates that echo top measurements must be made within a 100 nm (185 km) radius of the radar.

Another problem with non-digital radar observations is that it takes a finite amount of time to record the observation. This can amount to as much as twenty minutes in a complex weather situation. Therefore, a top height recorded at a particular time may have actually been measured significantly earlier. The GOES, particularly in a rapid scan mode, is a nearly instantaneous measuring device. The 250 lines are scanned in only 2.5 minutes. Thus, we have knowledge of the exact time of the measurement. Digital radar also provides an exact measurement time.

A large discrepancy occurred in echo top measurements at 2330 GMT observed by the St. Louis (STL) and Marseilles (MMO) radars. STL reported a top at 60,000 feet (18.3 km) while MMO reported a top at 50,000 feet (15.4 km). The satellite-derived height confirmed the MMO report at 50,000 feet. Other tops in the area were less than 50,000 feet. This suggests that satellite data could be used to verify radar reports that appear unusual in relation to other tops in the immediate area.

Many tops were observed in the satellite data that could not be correlated with echo tops reported in the radar logs and vice versa. This results from unreported radar echo tops as well as echoes which do not have a significant overshoot penetrating the cirrus anvil. However, the most severe storms will almost always penetrate the tropopause allowing for detection by satellite.

4.4 Overshooting Tops and Severe Weather Occurrences

4.4.1 Time-height variations

The time-height variations of overshooting tops have been shown to be correlated with the occurrence of severe weather on the ground. A brief discussion of several investigations relating to overshooting tops was presented at the beginning of this chapter. Almost all of the studies to date have relied on aircraft measurements to study these overshooting phenomena. An attempt is made in this study to examine overshooting top height variations prior to the occurrence of severe weather by using the shadow height estimation technique discussed in the previous section.

A time-height comparison of overshooting top heights just prior to severe weather occurrences is presented in Figure 4-9 and Figure 4-10. The tops associated with each severe weather occurrence are identified by the small mark at the end of each severe weather label. It should be noted that these top heights are measurements of penetrations above the cirrus anvil. No attempt was made to add them to the IR-determined height. This facilitates comparison with other studies.

It was possible to observe the overshooting top behavior prior to seven severe weather occurrences. The number was restricted due to the limited time in which shadows can be detected. The most obvious feature on the time-height plots is that tops associated with hail tend to be much higher than those associated with the occurrence of tornadoes. In every hail case, there was at least one top higher than any top associated with a tornado occurrence. The highest tops occurred just prior to or simultaneously with the occurrence of hail. The average height of the maximum tops associated with hail was 3.09 km while the average height of maximum tops associated with tornadoes was 2.05 km. Despite the time frequency of the data, it is very likely that much of the variation in top height cannot be seen. Also, it is very difficult to insure that the same top is being viewed on two successive images. For this reason no attempt was made to fit the points to a smooth curve.

The results from this limited sample tend to support previous investigations of overshooting top behavior using observations from aircraft. The extremely high tops associated with hail occurrence

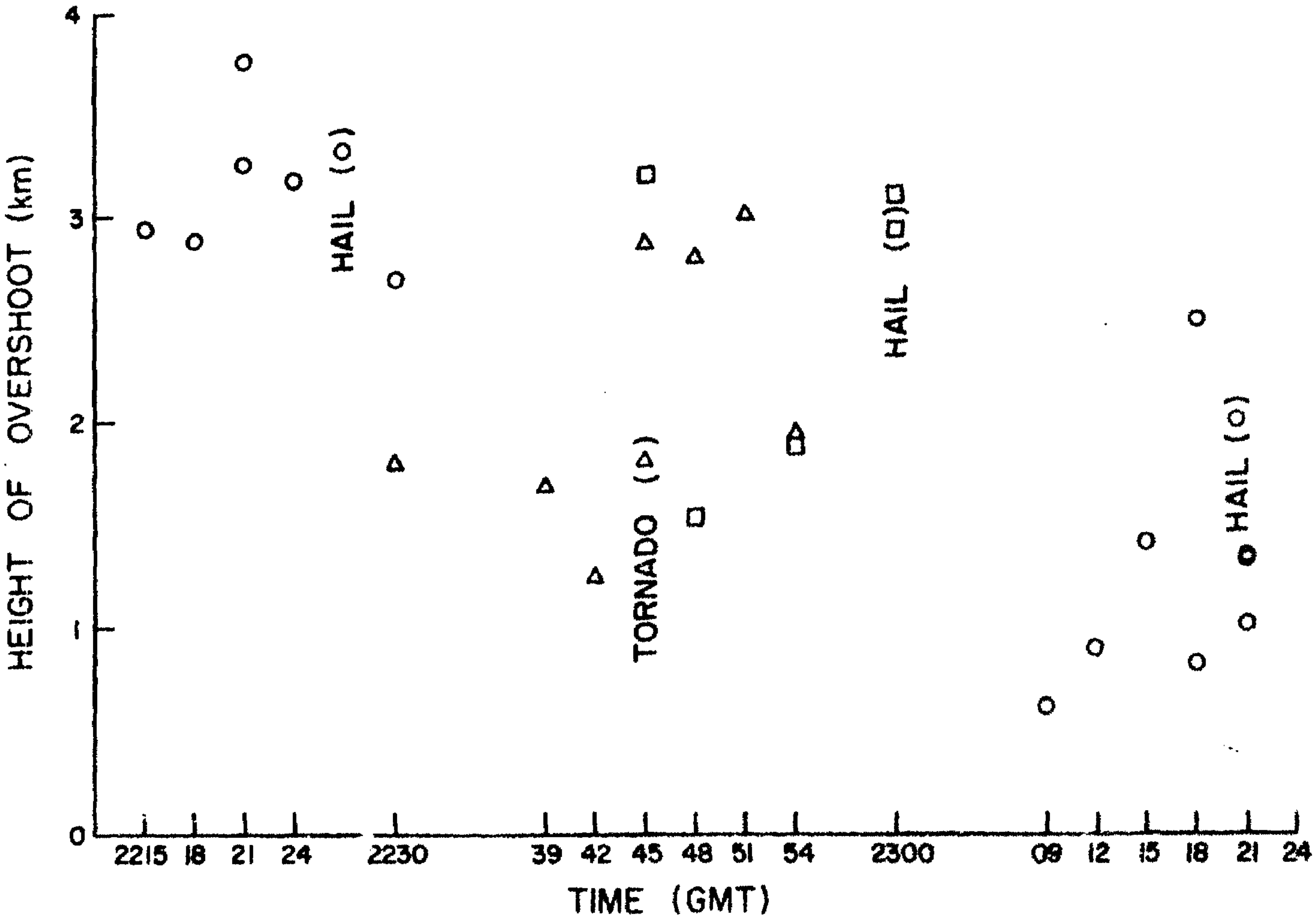

Figure 4-9 Time-height variation of overshooting tops (Missouri-Illinois area).

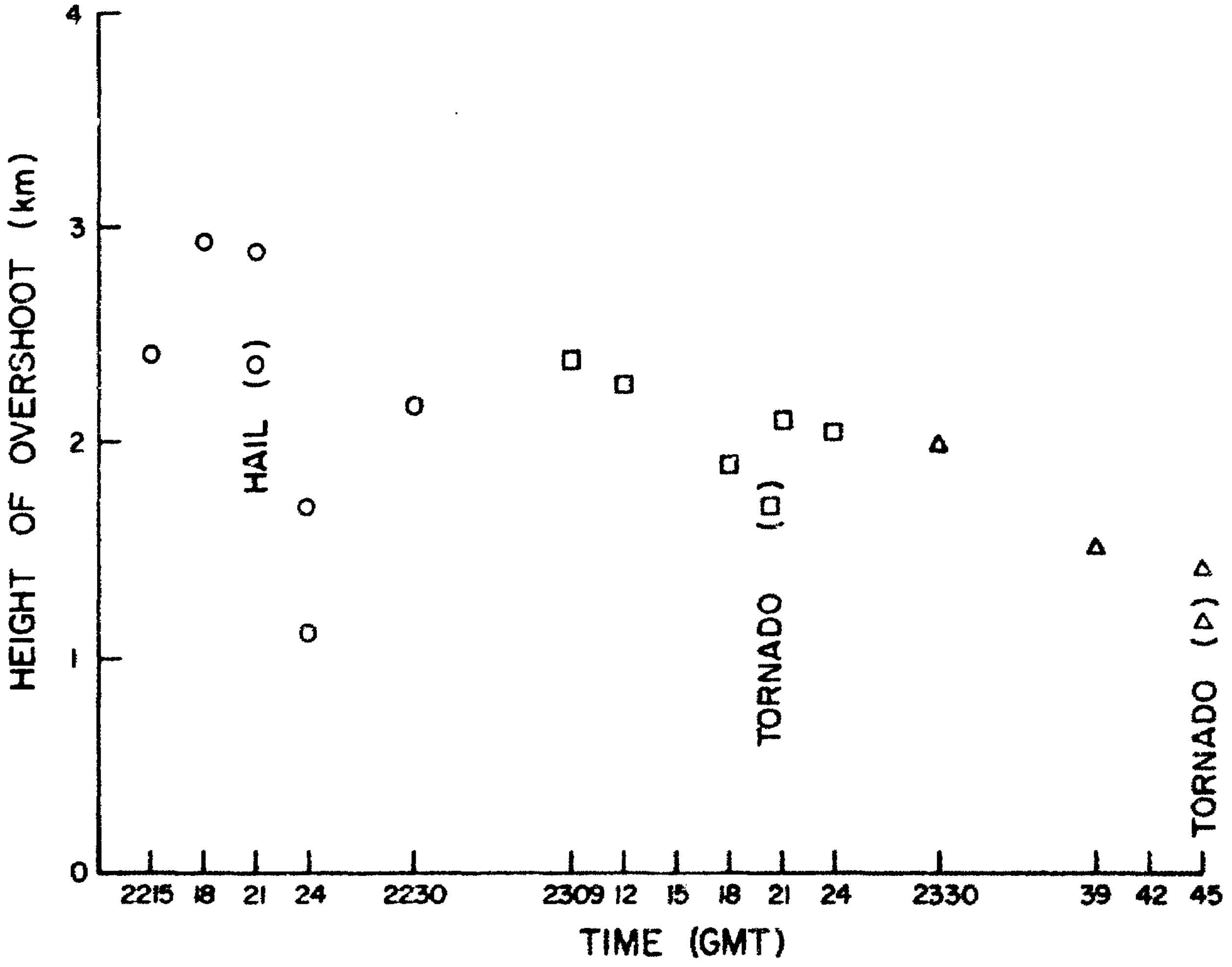

Figure 4-10 Time-height variation of overshooting tops (Kansas City-Topeka area).

reinforce the results of Pearl et.al. (1975). The observation that tornado-associated tops are somewhat lower than those associated with hail supports conclusions of Fujita (1972) and Umenhofer (1975). The heights of tornado-associated protrusions, however, were somewhat larger than those determined by Lee (1971).

From the data presented here it appears that overshooting tops associated with hail are distinguished by their large vertical extent. Little can be said about tops associated with tornadoes except that in this study heights prior to tornado occurrence were considerably lower than for hail. It is quite possible, however, that the observation of Bonner and Kemper (1971) is valid; that tornado occurrences are relatively insensitive to radar echo top height and consequently to overshooting top heights.

4.4.2 Visible and infrared imagery

Some examples of collocated visible and infrared imagery are displayed in Figures 4-11 through 4-20. It was necessary to go through this collocation process in calculating convective cloud heights presented in Section 4.2. The temperature values corresponding to the color enhanced areas in the IR are presented in Table 4-2. This enhancement is valid for all enhanced IR images in this paper. Severe weather reports corresponding to the image times are displayed on each image. This kind of display allows for a ready comparison between the visible and IR data.

From examining these photographs it becomes quite obvious that overshooting tops in the visible do not necessarily correspond to cold areas in the IR. The reports of tornadoes all occur outside the coldest

Table 4-2

Color Enhancement Values for Infrared Images

Color	Temperature (^{o}K)	Digital Count
Red	< 205	> 213
Green	206 - 208	212-210
Blue	209 - 211	211 - 209
Yellow	212 - 226	206 - 192
Gray shades	225 - 330	191 - 0

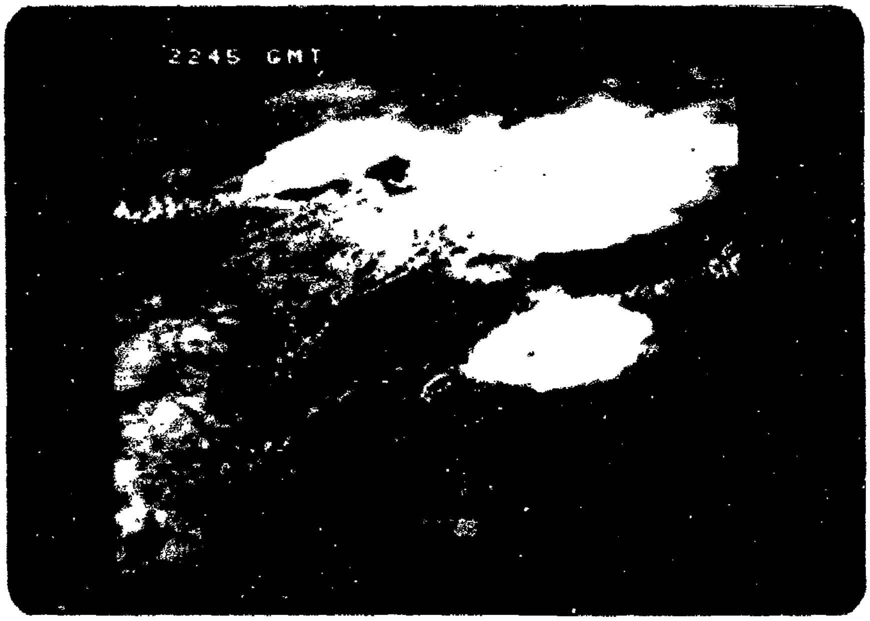

Figure 4-11 Visible image at 2245 GMT showing location of Middletown, IA tornado.

Figure 4-12 Infrared image at 2245 GMT showing location of Middletown, IA tornado.

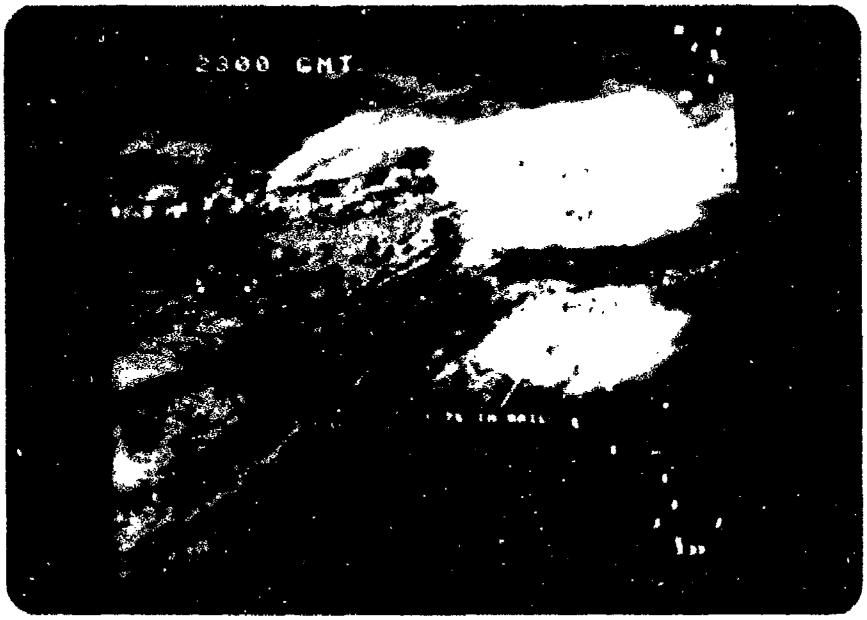

Figure 4-13 Visible image at 2300 GMT showing location of hail at Wentzville, MO.

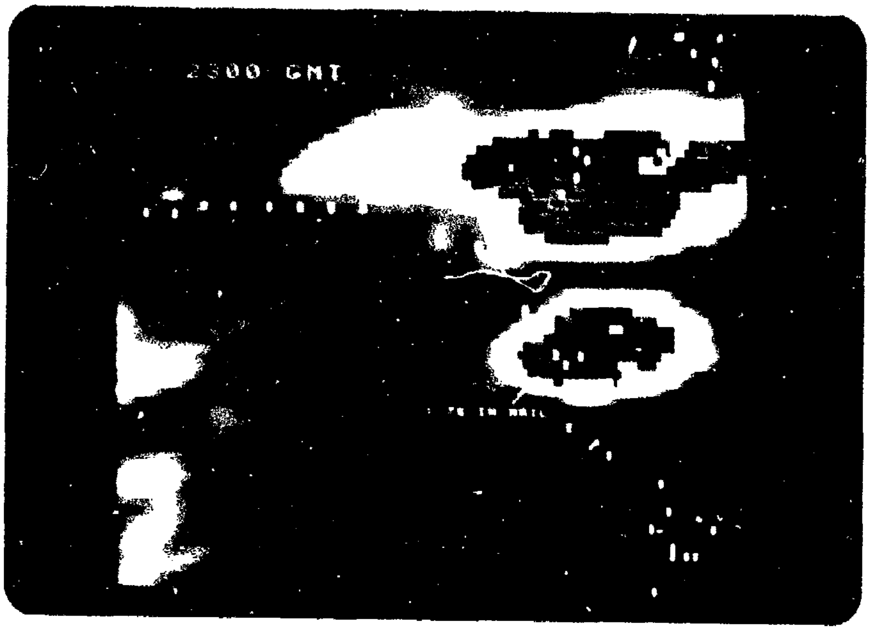

Figure 4-14 Infrared image at 2300 GMT showing location of hail at Wentzville, MO.

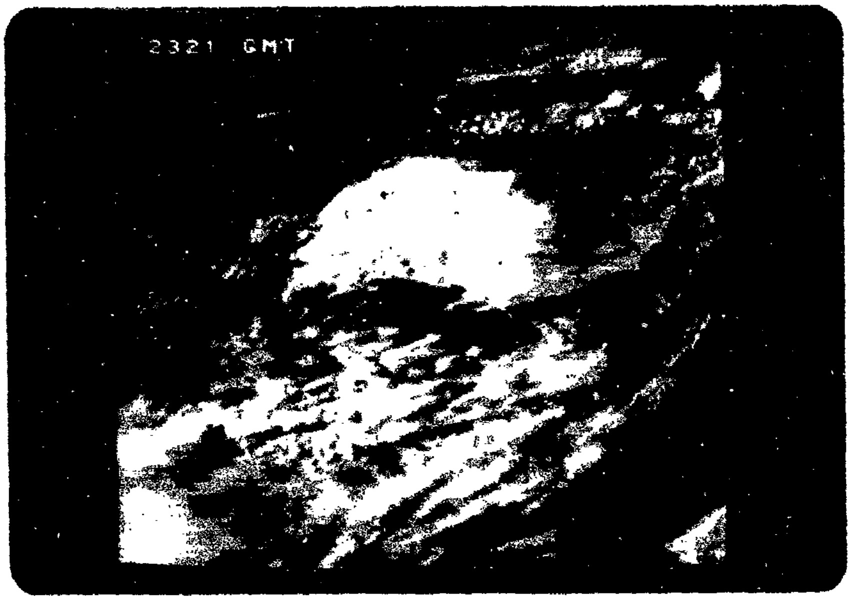

Figure 4-17 Visible image at 2321 GMT showing location of tornado at Weston, MO.

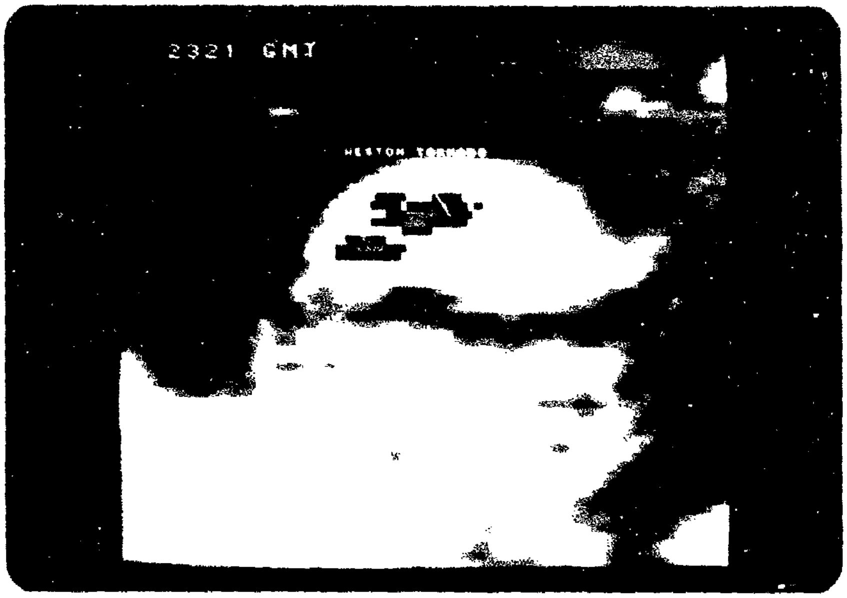

Figure 4-18 Infrared image at 2321 GMT showing location of tornado at Weston, MO.

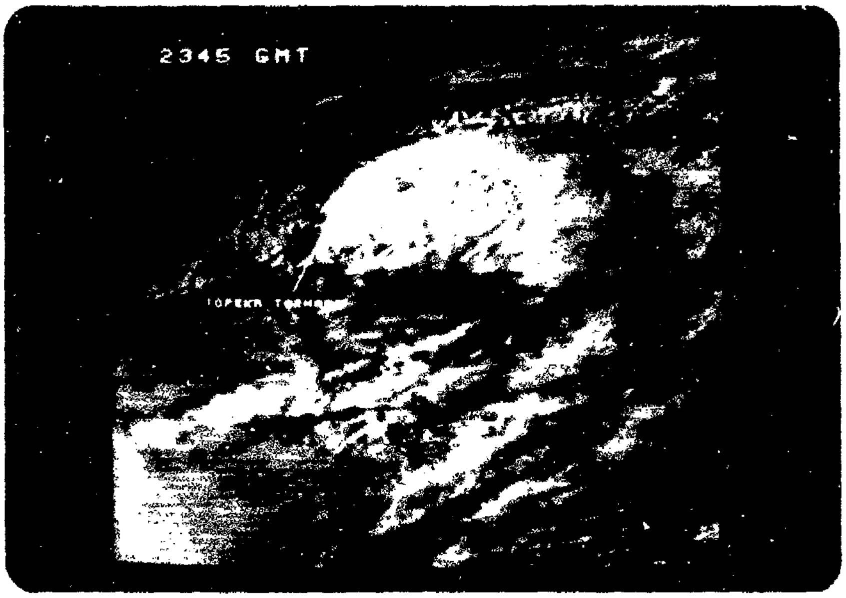

Figure 4-19 Visible image at 2345 GMT showing location of tornado at Topeka, KS.

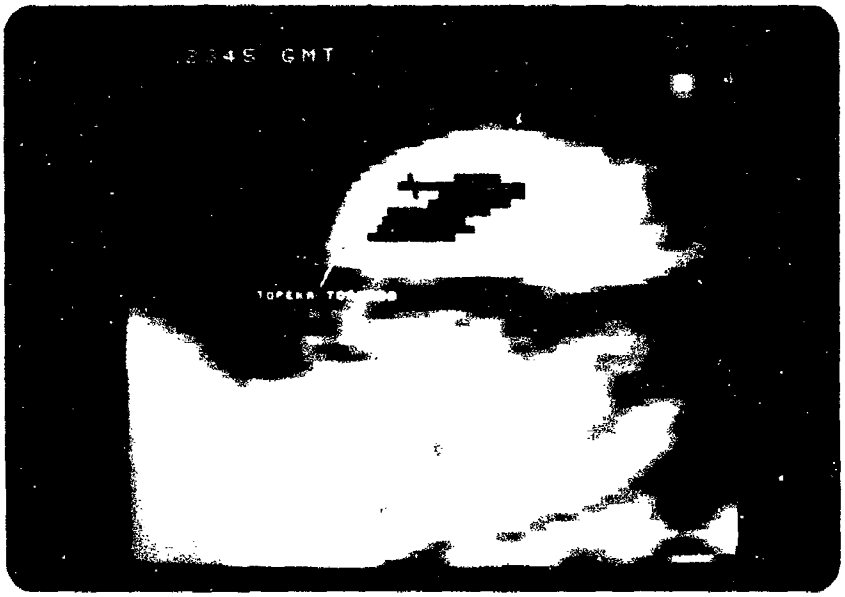

Figure 4-20 Infrared image at 2345 GMT showing location of tornado at Topeka, KS.

areas of the clouds. The hail reports appear to be closely associated with small cold areas and distinct overshooting tops. There were many observable overshooting tops, however, that had no closely associated severe weather. These images serve to illustrate the difficulty in determining where severe weather would occur simply be observing satellite imagery. They also show that overshooting tops cannot be reliably located using infrared imagery alone.

5.0 MONITORING OF THUNDERSTORM CLOUD-TOP PARAMETERS

A geosynchronous satellite is ideally suited to observe short-term variations in cloud motion. Large fields of view can be observed in near real time whereas radar observations, although excellent for local purposes, involve substantial errors when composited on a large scale. The time delay in such large scale compositing is critical when attempting to monitor convective cloud systems for a potential severe weather threat. Thus the development of severe storm monitoring techniques by satellite is of prime importance.

The most easily accessible information relating to cloud-top parameters is contained in the IR. Using the IR sensor of GOES-1, this study will explore differences between severe and non-severe storms and attempt to detect cloud-top signatures that would correlate with severe weather occurrences on the ground.

5.1 Previous Studies

The variation of cloud-top parameters can best be studied by a satellite with a high temporal resolution. Since these data first became available with the launch of the Applications Technology Satellite (ATS) several attempts have been made to correlate variations in cloud top parameters with severe weather occurrences.

Purdom (1971) used ATS imagery to measure growth rates in thunderstorm anvils. He noted that in two tornado-producing storms there was a pause in the rate of anvil growth near the time tornadoes occurred. A similar conclusion was reached by Fujita (1972). Studying anvil area increases and severe weather occurrences, he detected a tendency for tornadoes to weaken or die out as the anvil growth rate increases.

With the advent of the SMS/GOES series of satellites, infrared and higher resolution visible data became available. Arn (1975), using ATS and SMS visible imagery, determined three parameters that appear to be useful in examining severe storms. These were:

1) Area speed gradient $\left(\frac{d^2A}{dt^2}\right)$.
2) Volume flux $\left(\frac{dV_o}{dt}\right)$.
3) Divergence $(\nabla \cdot \vec{v})$.

Adler and Fenn (1976, 1977) used digital IR data from an SMS satellite to calculate thunderstorm growth rates and variations in cloud top structure. They concluded that three variables give indications of being correlated with tornadoes and hail. These are:

1) duration of a definable element below a temperature of 226^{o}K.
2) minimum cloud top temperature
3) logarithmic rate of increase of cloud top area.

Negri (1977) employed similar techniques to examine severe storms with high temporal frequency SMS IR data. His results were in general agreement with those of Adler and Fenn.

Examination of the variation in anvil growth rates has shown some promise in the detection of severe weather events. Unfortunately, due to the tremendous volume of digital satellite data required for a single case study, data samples must necessarily be limited in size. It is therefore essential to make as many contributions as possible to the base of data examined in this manner.

5.2 Description of Area Studied

Five separate areas of thunderstorm activity are examined in this study. The areas are depicted in a color enhanced IR image in Figure

5-1. The corresponding temperature values for each color are given in Table 4-2. The thunderstorm areas are labeled Cloud 1 through Cloud 5. This does not imply that these are individual thunderstorm cells since many isolated convective elements appear both in the visible satellite imagery and in radar scope photography. The areas, however, present fairly contiguous patterns in the IR and, as such, are easily studied. Clouds 2 and 3 produced no severe weather while Clouds 1, 4 and 5 were associated with several reports of hail and tornadoes.

5.3 Minimum Cloud-Top Temperatures

The minimum blackbody temperature of the anvil top of a thunderstorm is an easily measured parameter which provides a source of information about storm severity. The blackbody temperature changes for Clouds 1-5 are given in Figure 5-2. Times of occurrence of severe weather events are shown for each cloud. The non-severe storms show a marked difference from the severe storms in their life history. The non-severe storm tops are never colder than 214° K, while the severe storms all reach at least 205° K with Cloud 5 reaching a minimum of 201°K, the lowest temperature detected in the data set. No severe weather was associated with minimum temperatures higher than 211° K (Cloud 4 at 2224 GMT).

One of the more interesting features in Figure 5-2 is that no severe weather was reported until the minimum temperatures of the severe storms were 4-5° K less than those of the non-severe storms. This suggests that storms which have the potential for severe weather can be identified prior to the actual occurrence of hail or tornadoes by the determination of a threshold temperature.

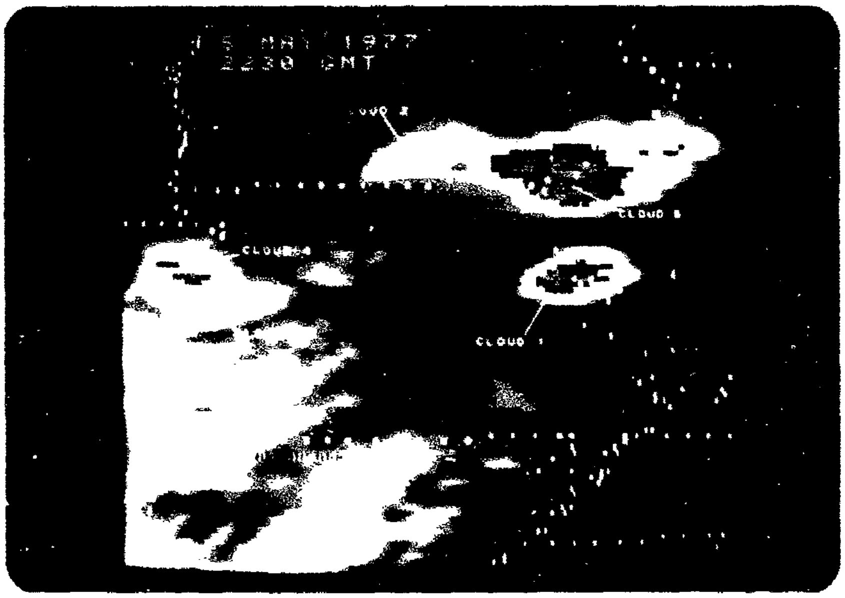

Figure 5-1 Infrared image at 2230 GMT indicating clouds studied.

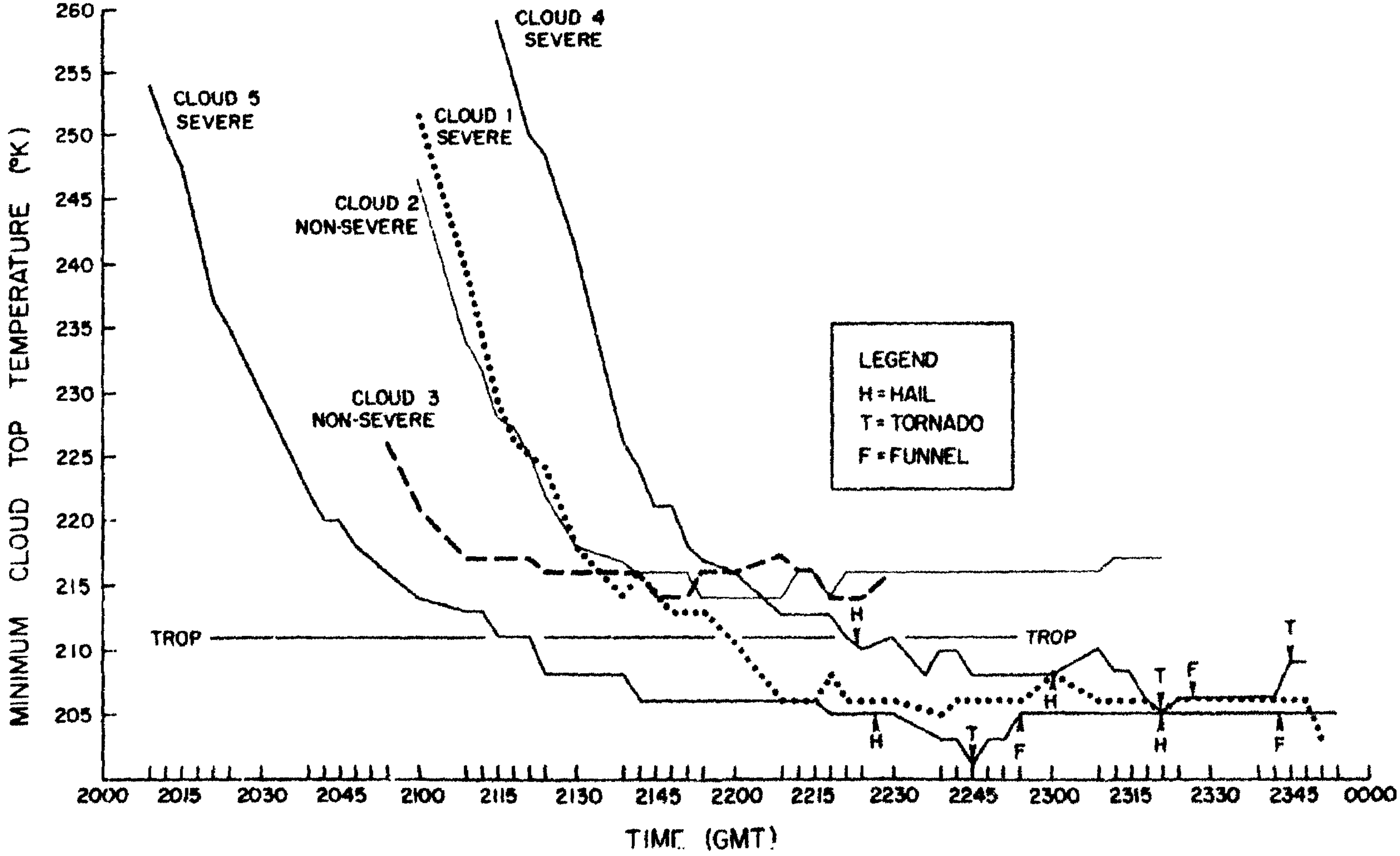

Figure 5-2 Variation in blackbody temperature for three severe and two non-severe storms.

Severe storms would be identified by minimum cloud-top temperatures lower than the threshold value. All severe weather was reported when the minimum temperature was less than the environmental tropopause temperature. This suggests that the tropopause temperature might be a good first guess as a threshold value. Minimum temperatures of Clouds 2 and 5 were lower than the tropopause temperature for approximately one hour before any severe weather was reported while Cloud 4 had a severe weather report three minutes after reaching the tropopause value. It is possible that some lead time might be available with which to identify potentially severe storms. However, it is hard to tell without a larger data sample. It does appear, though, that the minimum blackbody temperature of an anvil top is important in identifying thunderstorms which produce severe weather.

5.4 Thunderstorm Growth Rates

Thunderstorm cloud-top divergence as measured by the expansion of the cirrus anvil has been shown to be important in identifying storms which have severe weather potential (Sikdar et.al., 1970; Adler and Fenn, 1976, 1977; Negri, 1977). Horizontal cloud divergence D_c, is related to the change in cloud area A through the equation

$$D_c = \frac{1}{A}\frac{dA}{dt}. \tag{5-1}$$

Following methods outlined by Adler and Fenn, areas of the cloud top colder than a certain blackbody temperature T_{BB} can be defined. The number of IR pixels, N, colder than T_{BB} can be substituted for the areas in Equation (5-1).

$$D_c = \frac{1}{N}\frac{dN}{dt} \qquad (5\text{-}2)$$

The procedure for calculating cloud areas using the ADVISAR is relatively simple. A box-like cursor is overlayed on an IR image displayed on the video monitor. The cold top of a thunderstorm cell is surrounded and a histogram of digital counts within the cursor is printed out. The digital counts are then converted to temperature values. A cumulative histogram is then prepared starting with the lowest temperature.

In the range of digital counts examined at cloud top (192-217) it is possible to obtain a 1° K resolution. However, due to a problem in the transfer of raw counts to calibrated values, some counts never appear. These missing counts occur at intervals of every 3 to 5 counts.

Growth rate diagrams for Clouds 1, 2, 4, and 5 are shown in Figures 5-3 through 5-6. Cloud 3 is not presented because the early stages of its growth were not visible due to cirrus overcast. The early portions of growth for Cloud 5 are not shown because the area formed simultaneously from at least five separate convective cells. Thus, no attempt will be made to correlate initial growth rates with severe weather occurrences. The slope of the lines is a measure of divergence.

Cloud 1 (Figure 5-3) was an extremely fast-growing thunderstorm which formed just to the west of St. Louis, Missouri. The single report of severe weather, 1.75 in. (4.4 cm) hail at Wentzville, Missouri, occurred at 2300 GMT, almost two hours after the storm first appeared. Several interesting features present themselves on the growth rate diagram. After a period of rapid initial growth and the appearance of temperatures of 208° K and 206° K at 2209 GMT, both temperatures

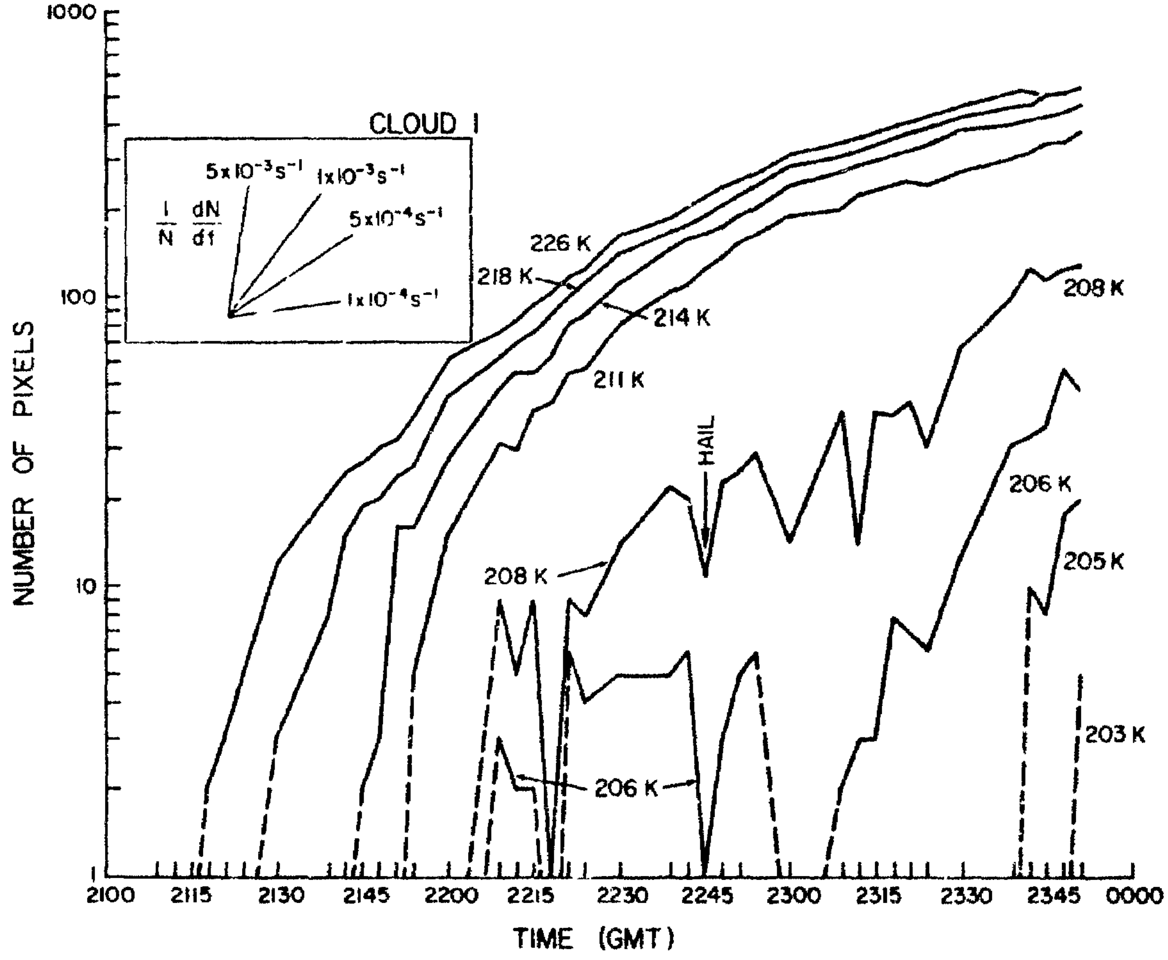

Figure 5-3 Growth rate diagram for Cloud 1.

completely disappear at 2218 GMT, then reappear at 2221 GMT. It is difficult to think of a physical reason for such an occurrence, thus, it is likely such fluctuations are noise in the data. The report of hail occurs simultaneously with a similar dip in the 208° K temperature area and follows a period of sharp increase in the coldest areas (206° K and 208° K). The growth rate becomes quite rapid once again following the hail occurrence.

An example of a non-severe storm, Cloud 2 (Figure 5-4) differs markedly from Cloud 1 in several respects. Although the initial growth rates are similar for the 226° K and 218° K areas, there was no subsequent development of areas colder than 214° K. The growth of the 226° K area quickly leveled off then decreased indicating the cloud-top divergence was zero implying that the cloud updraft had ceased.

Cloud 4 (Figure 5-5) formed just to the south of Topeka, Kansas, 2130 GMT. Its initial growth rate is similar to that of Cloud 1. Hail was first reported at 2220 GMT after the period of initial rapid growth. At 2242 GMT new development became apparent to the west of the original cell. By 2318 GMT, two separate cold elements could be defined. The oldest element, denoted as "east" on the growth rate diagram was associated with a tornado at Weston, Missouri, at 2320 GMT. This was accompanied by the appearance of a 206° K area which subsequently disappears. In the western area a funnel occurred at 2327 GMT and a tornado was reported at Topeka, Kansas, at 2345 GMT. The tornado occurs simultaneously with the disappearance of the 206° K area. This area did not return prior to 2400 GMT.

As a final example of a severe storm, Cloud 5 growth rates are presented in Figure 5-6. This storm formed at 2000 GMT, earlier than

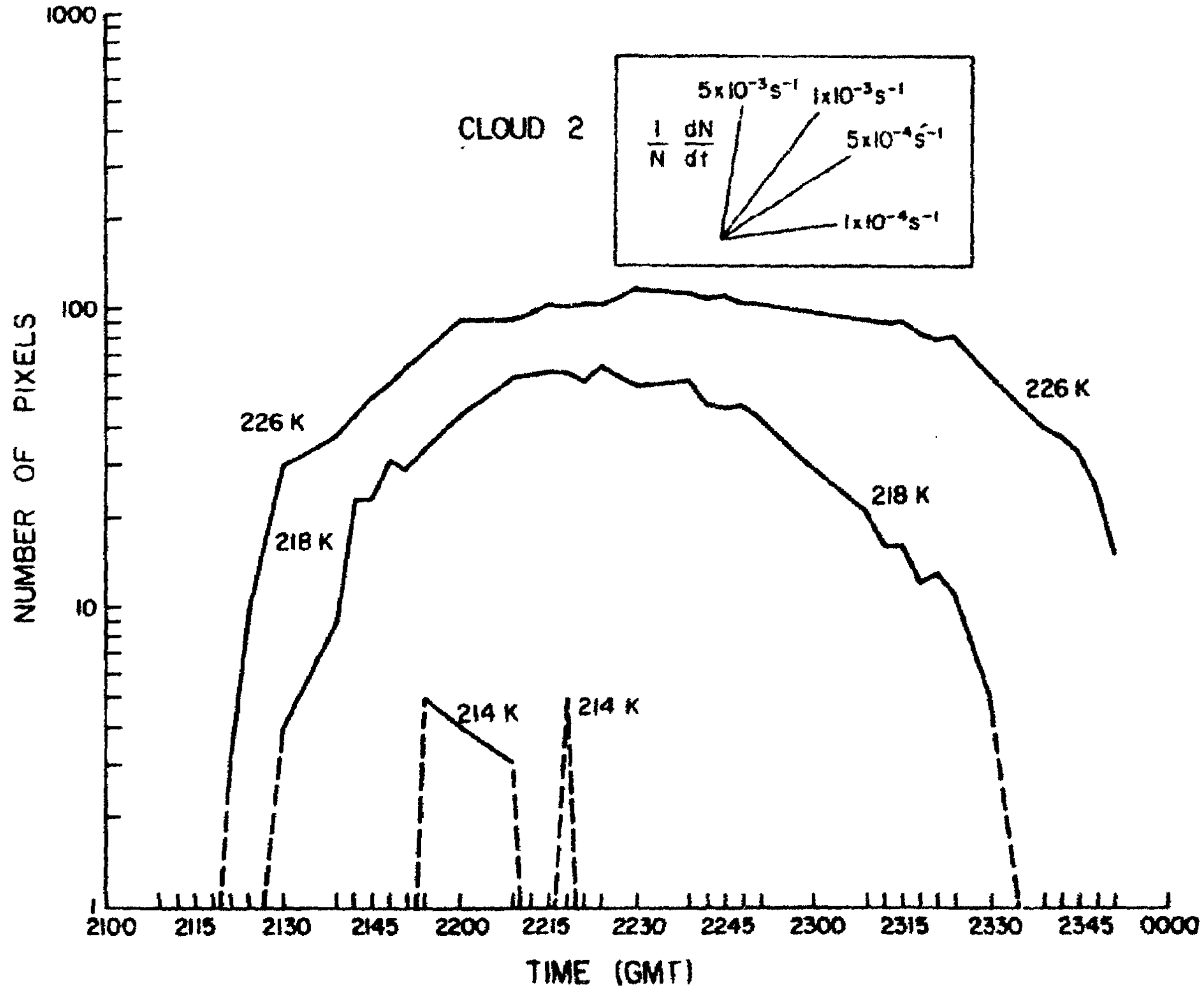

Figure 5-4 Growth rate diagram for Cloud 2.

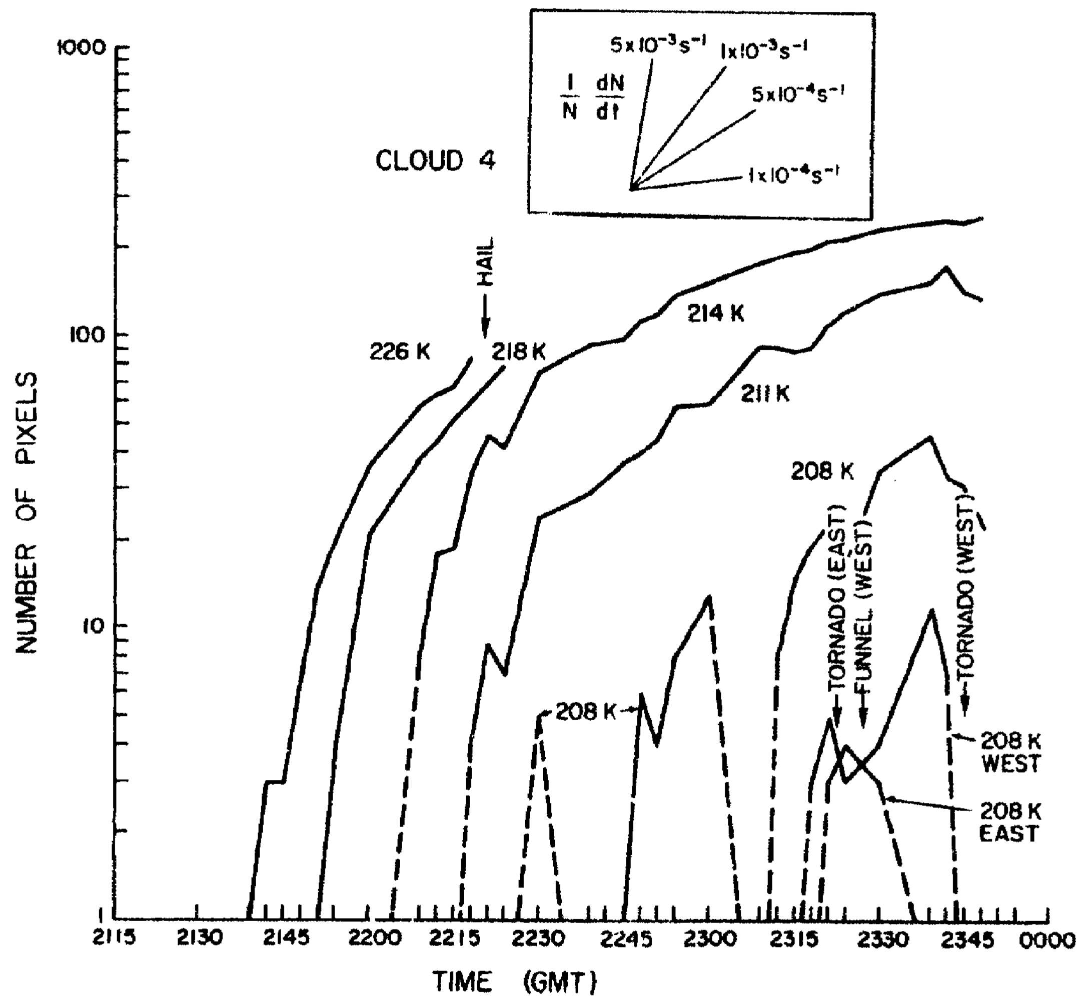

Figure 5-5 Growth rate diagram for Cloud 4.

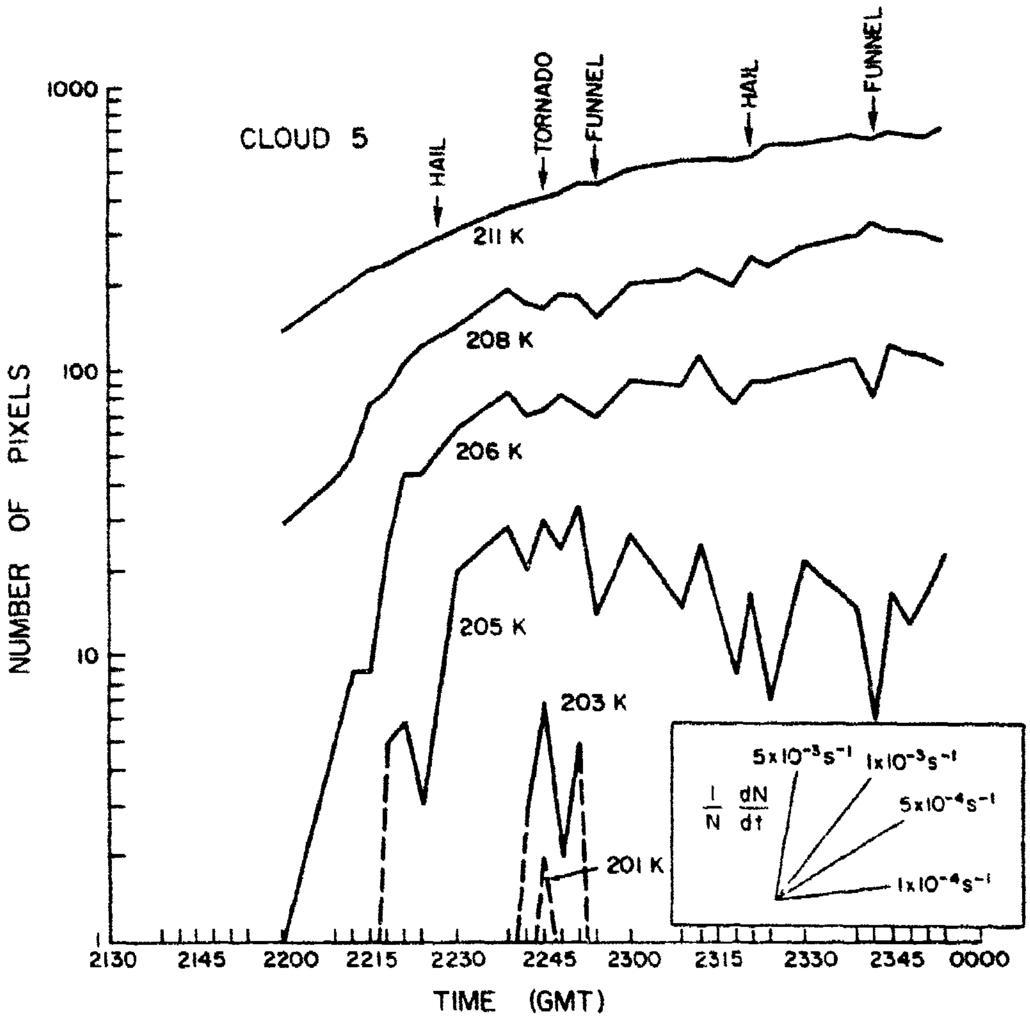

Figure 5-6 Growth rate diagram for Cloud 5.

any other, and grew as a multi-cell complex. The first occurrence of severe weather was 1 in. (2.5 cm) hail at 2227 GMT, well after initial storm formation. Subsequent reports included a tornado at 2245 GMT, a funnel at 2254 GMT, 1.75 in. (4.4 cm) hail at 2320 GMT and another funnel at 2343 GMT. The tornado, which was confirmed by the radar observation of a hook echo, occurred simultaneously with the appearance of a very cold area (201° K). However, this tornado and the two funnel reports occurred when pauses in the growth of larger areas (208° K, 206° K) took place. This particular storm was difficult to observe due to its multi-cell nature. There were numerous convective elements which had no separable IR signature from other elements. All severe storms in the area were of multi-cell nature at some time during their life span.

The growth rate diagrams for the three severe storms examined here demonstrate little in the way of signatures that would be a key to occurrences of severe weather. Adler and Fenn (1977) found that the first report of severe weather occurred during, or just after, a rapid expansion of cold areas. Except for Cloud 4 it was hard to find any such relationship. The occurrence of tornadoes seemed to be associated with the appearance of the coldest areas of the cloud. However, it is unlikely that this could be used as an indicator of impending tornadic activity since these cold areas occur simultaneously with the tornadoes.

6.0 IMAGE DIFFERENCING

The capabilities of the ADVISAR allow for several pixel-for-pixel operations between two images stored in the memories. These include average, maximum, minimum, and differencing functions. The resultant images of these operations contain information about cloud growth and advection. The differencing function will be explored in this chapter.

Previous studies in the area are limited due to the specialized electronics required. Serebreny et.al. (1970) demonstrated a frame-to-frame differencing technique using ATS imagery in which two images of different times were overlayed. The earlier image had been reversed in brightness so that clouds appeared dark. The resultant overlay showed areas of increased brightness in white and areas of decreased brightness in black. Reynolds et.al. (1978), using the advanced capabilities of the ADVISAR, utilized image differencing to differentiate between cloud types by differencing collocated visible and IR SMS data. This technique emphasized the identification of cirrus and the differentiation of snow from clouds.

6.1 Method

Pixel-for-pixel differencing between two images of different times provides a resultant image which contains information on either cloud motion, cloud growth, or both. Utilizing three-minute interval satellite data provides a unique opportunity for using differencing to explore very short-term cloud variations.

The first requirement in differencing two images is that the images be precisely registered to geographic landmarks. This procedure is discussed in Chapter 3. If the images are precisely registered the resultant image will show any misalignment as motion.

After registration, the pixel-for-pixel differencing is accomplished by actually subtracting brightness values of an image at time t from an image at time t+1. Resultant values are calculated by

$$\frac{B_{t+1} - B_t}{2} + 127 = B_r \qquad (6\text{-}1)$$

where: B_{t+1} - brightness values at time t+1.

B_t - brightness value at time t.

B_r - brightness value of the result.

This operation produces images in which gray areas represent little or no change, white areas indicate brightness (cloud) increases, and dark areas show brightness (cloud) decreases. This type of image contains information that can be extracted through additional processing.

The no-change range of counts is identified by obtaining a histogram of counts of an area that is known not to change. Such an area is cloud free land. Some brightness changes will occur due to variation in the sun angle with time and from noise in the data. Thus a spectrum of counts is obtained from the no-change area. This spectrum is illustrated in Figure 6-1. The values are obtained from a difference of two images three minutes apart in time. The number of counts were normalized to the maximum value which occurred at count 127. The entire spectrum was contained between counts of 119 and 135. There are no even-valued counts since the differencing algorithm assigns resultant counts to an odd number.

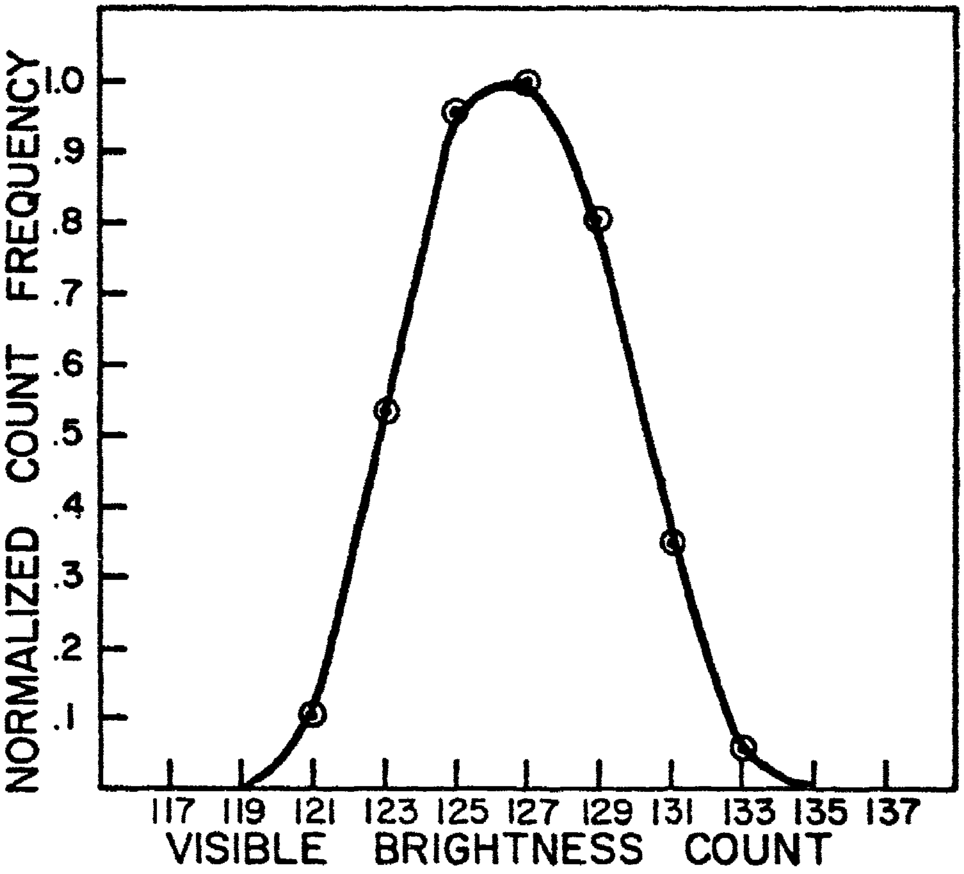

Figure 6-1 Spectrum of counts for no-change area.

The image is then processed into a three-valued image by using the boundaries of the no-change spectrum as dividing points. This procedure divides the image into three sections each of which has one value. The sections are:

1) white; areas that have increased in brightness
2) gray; areas in which little or no change has taken place
3) black; areas in which the brightness has decreased.

The white areas signify regions in which clouds have either been advected or developed. The gray areas are regions in which there has been no change, whether covered by clouds or not. The black areas signify regions in which clouds have been reduced.

With the areas so quantified it is possible to surround a given cloud or cloud group with the cursor and obtain a histogram of values. The three values obtained, N_W, N_G, N_B, are the number of pixels representing the white, gray, and black regions respectively. Since these values represent areas of each region, ratios of the two numbers may be formed to give a quantitative measure of the cloud growth, dissipation or advection in each area. For example, if $\frac{N_W}{N_B} > 1$ there would be a net areal increase of clouds. If one is cognizant of the type of cloud being observed, this can be a measure of growth. Such a cloud could be a rapidly developing thunderstorm. Similarly, if $\frac{N_W}{N_B} \sim 1$ and N_G was very large compared to N_W and N_B, we would expect little growth or advection.

It is very important in this procedure for a subjective determination of cloud type and cloud area to be made. Cloud shadows will show up as black areas on the difference image if such a shadow advects along the ground ahead of a fast moving cloud. In order to be useful, developing areas must be examined. A severe thunderstorm may be extremely active but its top will show up as gray in a short-term difference. It is the advancing anvil edge that contains the information.

6.2 Application

To demonstrate the image differencing technique, three perfectly registered images were chosen. The images at 1942 GMT, 1945 GMT and 1948 GMT show an area of west central Texas (Figures 6-2 to 6-4) where intense convective storms were taking place. For reference Midland, Texas (MAF) and Lubbock, Texas (LUB) are located on each image. The most striking feature in the area is a rapidly developing thunderstorm just to the south of Midland. The area also contains numerous storms which have formed broad anvil tops, areas of small cumulus, as well as fairly rapidly moving mid-level clouds. Several types of clouds are represented in the sequence of images.

Difference images were formed by subtracting the 1942 GMT image from the 1945 GMT image and by subtracting the 1945 GMT image from the 1948 GMT image. The two resultant images are displayed in Figures 6-5 and 6-7. The fast-developing thunderstorm is seen in both differences as a light region just south of Midland. The darker band just to the right of the light band is caused by the advection of the shadow that this cloud is casting on the ground.

Next, the two difference images are divided into images of three brightness values which represent increase (white), no-change (gray), and decrease (black) of brightness. These images are displayed in Figures 6-6 and 6-8. The dividing points for the three areas were determined by the method discussed in the previous section. It is readily apparent that the cirrus tops of well-developed thunderstorms

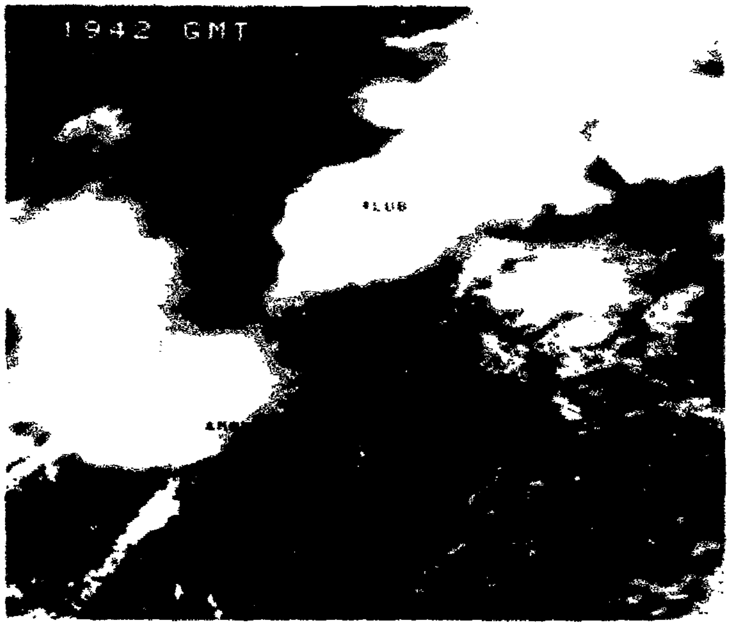

Figure 6-2 Visible image at 1942 GMT.

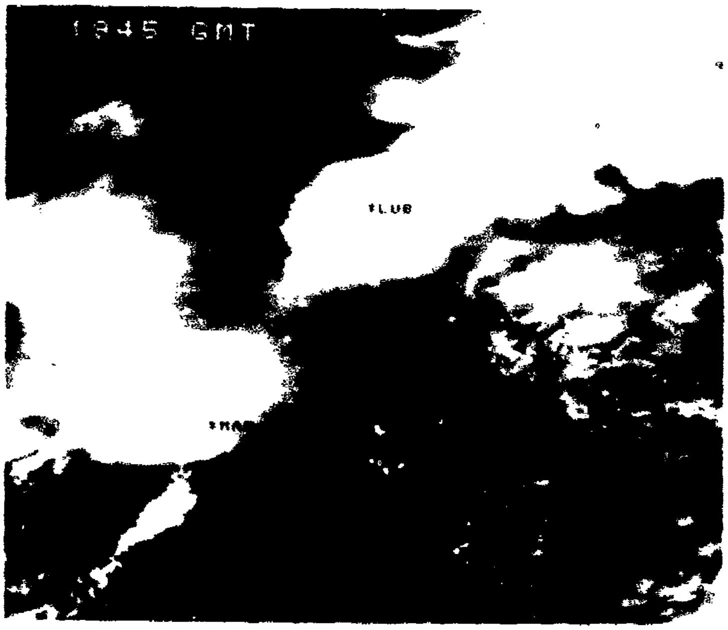

Figure 6-3 Visible image at 1945 GMT.

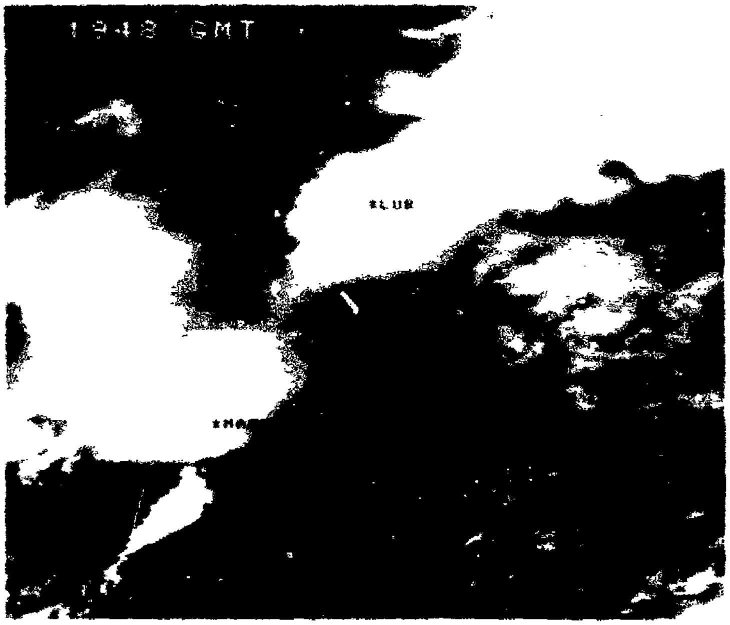

Figure 6-4 Visible image at 1948 GMT.

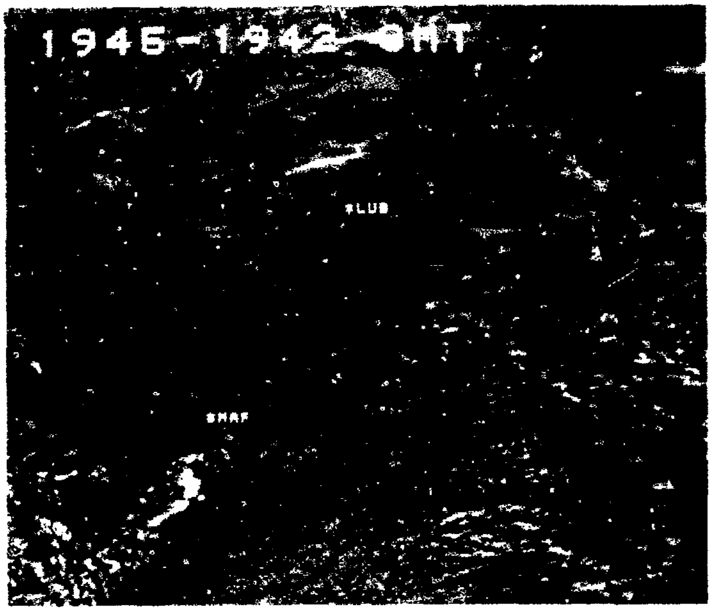

Figure 6-5 Difference of 1945 and 1942 GMT images.

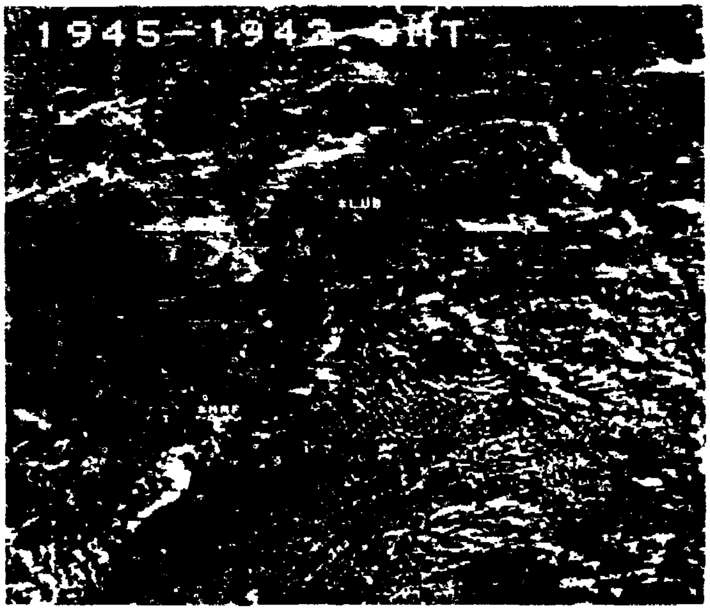

Figure 6-6 Three-valued 1945-1942 GMT image.

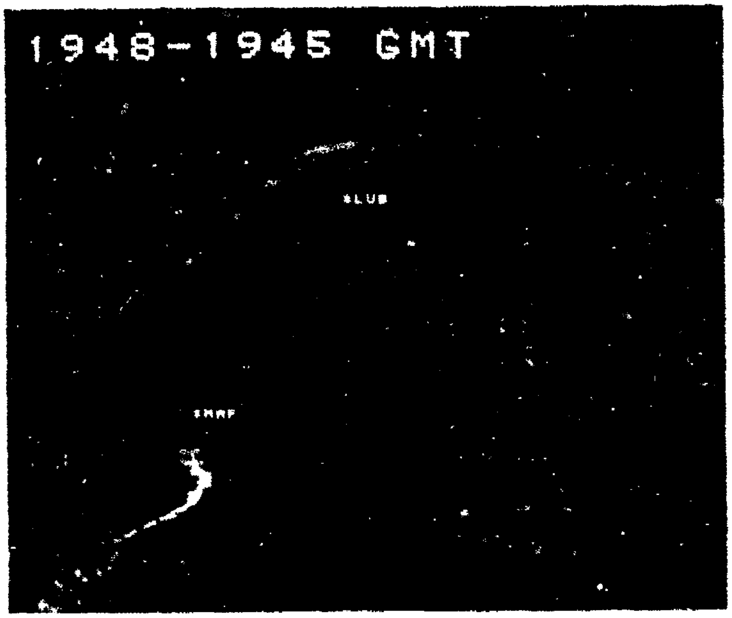

Figure 6-7 Difference of 1948 and 1945 GMT images.

Figure 6-8 Three-valued 1948-1945 GMT image.

show up almost entirely gray. Examples of this type of cloud are located near Midland and Lubbock. Ground areas show up as gray as one would expect.

The three-valued images were divided up into boxes of 64 rows x 64 columns using the cursor. An entire image contains 64 such boxes, however, only the lower half of each image was gridded. A histogram of each image was obtained and the fractional values for each image were calculated (Figures 6-9 and 6-10). Decrease (top), no-change (middle), and increase (bottom) values are given for each box. Reference to the grid boxes is made by row and column number respectively.

The most obvious feature is that the no-change values are largest in every case. The highest values of no-change are in boxes 4-1 through 4-4 in both grids. This area is the large cirrus anvil just north of Midland. The lowest values of no-change are generally in the upper right portion of the grids. Values of increase and decrease are about equal in this area. This implies that clouds in this area are simply being advected by the prevailing wind. Two grid boxes which contain the rapidly developing thunderstorm south of Midland, 2-2 and 2-3, both show comparatively large values of cloud increase compared to cloud decrease. This implies that some kind of development is taking place in the boxes and this can be readily observed in the visible images (Figures 6-2 and 6-4). No-change values are large here because much land area is contained in the boxes. A large ratio of decrease to increase is found in box 2-1 of Figure 6-10. In this case clouds were advected out of the box with no replacement from elsewhere. This box shows a similar ratio of decrease to increase in Figure 6-9.

	1	2	3	4	5	6	7	8
4	.061 .857 .081	.022 .915 .064	.007 .894 .099	.029 .807 .164	.208 .592 .199	.328 .408 .265	.282 .420 .298	.240 .440 .320
3	.215 .639 .146	.195 .705 .099	.137 .715 .149	.114 .754 .132	.138 .651 .211	.189 .555 .256	.289 .453 .261	.278 .476 .249
2	.156 .659 .187	.097 .690 .213	.066 .818 .115	.085 .827 .089	.136 .708 .157	.298 .414 .287	.161 .638 .201	.343 .530 .128
1	.217 .699 .085	.040 .881 .080	.096 .772 .132	.151 .705 .144	.202 .595 .203	.140 .729 .131	.222 .570 .208	.161 .673 .166

Figure 6-9 Grid of lower half of three-valued 1945-1942 GMT difference image showing fractional areas of decrease (top), no-change (middle) and increase (bottom) in clouds for each grid block.

	1	2	3	4	5	6	7	8
4	.052 .891 .056	.013 .938 .048	.005 .947 .048	.007 .879 .113	.139 .731 .130	.302 .485 .212	.251 .502 .247	.197 .555 .248
3	.163 .722 .115	.162 .770 .067	.084 .751 .165	.121 .797 .082	.143 .705 .152	.181 .631 .188	.276 .530 .188	.279 .569 .158
2	.138 .735 .127	.102 .762 .136	.074 .786 .140	.066 .872 .062	.118 .784 .098	.265 .531 .204	.132 .695 .173	.327 .607 .065
1	.246 .485 .269	.097 .790 .111	.088 .829 .083	.181 .725 .095	.187 .693 .121	.107 .783 .109	.186 .692 .122	.179 .722 .099

Figure 6-10 Grid of lower half of three-valued 1948-1945 GMT difference image showing fractional areas of decrease (top), no-change (middle) and increase (bottom) in clouds for each grid block.

This technique demonstrates a quantitative method of measuring cloud growth and advection. Advection is detected when values of increase and decrease are nearly the same. Cloud growth is detected when the cloud increase value is larger than the decrease value. One drawback in separating growth regions from advection areas is that a cloud advected into a box will look like growth when the areas are calculated. Thus, some care must be taken when calculating cloud areas. It would probably be easier to ascertain a good measure of cloud growth in a situation that is not as complex as the one presented here. However, it is the complex cloud situations that frequently produce severe weather. This method has the ability to detect rapidly growing cloud areas but this can easily be accomplished by calculating IR growth rates. Further research is indicated in the area of image differencing to explore all of its possibilities.

7.0 SUMMARY AND CONCLUSIONS

High-frequency satellite images were analyzed using the capabilities of the ADVISAR. Thunderstorms were examined in several ways to determine cloud-top signatures which might be correlated with severe weather occurrences.

Two methods of determining convective cloud-top heights were compared to measurements of radar echo tops penetrating the tropopause. Using the infrared sensor of GOES, maximum cloud-top heights were consistently underpredicted when compared to corresponding radar measurements of echo tops. When an overshooting top can be seen in the visible, its height can be calculated from the shadow cast on the cirrus anvil. When this height is combined with an IR-determined height, improvement is noted over the IR method alone. In one case it was possible to discriminate between two differing radar measurements of the same echo. A particular drawback to the shadow method is that it was accurate for only about one and a half hours (solar zenith angles between 60° and 75°) for this case.

The shadow method was used to study overshooting top behavior just prior to and during severe weather occurrences. Average maximum overshoots occurring with hail were 3.1 km while for tornadoes the maximum overshoots were 2.1 km. Even though the sample size was small this result was consistent with other studies.

Collocated visible and infrared imagery were displayed at the time of several severe weather occurrences. The images demonstrated that overshooting tops observable in the visible cannot necessarily be located as cold areas in the IR. The implication is that IR data alone is not sufficient to precisely locate areas of intense convection. Occurrences of hail seem reasonably well collocated with cold elements in the IR and overshooting tops in the visible. Tornado occurrences exhibit no such tendency.

Using methods developed by Adler and Fenn (1976, 1977) variations in the cloud tops of five thunderstorm systems were examined. Three of the storms produced severe weather and two were non-severe. Minimum cloud-top temperatures, as sensed in the IR, appear to be a good discriminator between severe and non-severe storms. No severe weather occurred until the minimum cloud-top temperature was less than that of the tropopause. Variations in IR growth rates of the storms were of little value in predicting times and types of severe weather occurrences.

As a method of quantitatively displaying the change in clouds over a specified time interval, an image differencing technique was examined. Qualitatively, difference images demonstrate regions of very rapid growth and expansion as a bright area. The larger and brighter the area the faster and more intense the change. The difference images were gridded and the relative change areas of each block were calculated. This offers a quantitative method of examining growth and advection.

Satellite data sets can be analyzed with comparative ease using systems such as the ADVISAR. There is no substitute for being able to interact qualitatively and quantitatively with satellite imagery. A man-interactive video display system is essential i developing techniques in the study of severe weather and it is mandatory for any meaningful operational use of high-frequency satellite data.

8.0 SUGGESTIONS FOR FURTHER RESEARCH

High-frequency satellite data sets such as the one analyzed in this study offer promise in detecting and monitoring severe storms. However, we are some distance away from operational use. It is not yet clear that operational monitoring of severe storms will allow a meteorologist to accurately predict in time and space where severe weather will occur.

The monitoring of overshooting tops is severely restricted due to the limited amount of time that shadows are observable. An important area of research would be the development of a method to detect and quantitatively measure overshooting tops at any time during the day. Since the IR is inadequate to reliably detect overshoots, visible data would have to be used.

Since such systems as the ADVISAR have the capability to handle any digital data sets, research is indicated on the combining of satellite and radar images. Such research would aid in the understanding of the relative positions of the lowest cloud-top temperatures and overshooting tops to the most intense radar echoes. In this way something might be learned about cloud dynamics in relation to the radar precipitation echoes and what variations in cloud-top parameters really mean in relation to severe weather.

Further research into image differencing techniques is also indicated using both visible and infrared imagery. This method could prove to be a valuable way of detecting subtle changes in cloud brightness over a short time interval.

REFERENCES

Adler, R. F. and D. D. Fenn, 1976: Thunderstorm monitoring from a geosynchronous satellite. Preprint of Seventh Conf. on Aerospace and Aeronautical Meteorology and Symposium on Remote Sensing from Satellites, AMS, Melbourne, Florida, 307-311.

Adler, R. F. and D. D. Fenn, 1977: Satellite-based thunderstorm intensity parameters. Preprint of Tenth Conf. on Severe Local Storms, AMS, Omaha, Nebraska, 8-15.

Arn, R. M., 1975: Anvil area and brightness characteristics as seen from geosynchronous satellites. Master's Thesis, Colorado State University, Fort Collins, Colorado, 88 p.

Bonner, W. D. and J. E. Kemper, 1971: Broad-scale relationships between radar and severe weather reports. Preprints of Seventh Conf. on Severe Local Storms, AMS, Kansas City, Missouri, 140-147.

Brown, M. L., 1978: Digital video manipulation of satellite data. Preprint of Fourth Symposium on Meteor. Observations and Instrumentation, AMS, Denver, Colorado, 207-211.

Cox, S. K., 1977: Satellite derived cloud-cluster cloud-top heights. Volume of Conference Papers: Eleventh Technical Conference on Hurricanes and Tropical Meteorology, AMS, Boston, Mass. 355-356.

Donaldson, R. J., 1964: A demonstration of antenna beam errors in radar reflectivity patterns. J. Appl. Meteor., 3, 611-623.

Fujita, T. T., 1972: Tornado occurrences related to overshooting cloud-top heights as determined from ATS pictures. SMRP Research Paper 97, University of Chicago, 32 p.

Fujita, T. T., 1974: Overshooting thunderheads observed from ATS and Learjet, SMRP Research Paper 117, University of Chicago, 29 p.

Galway, J. G., 1956: The Lifted Index as a predicator of latent instability. Bull. Amer. Meteor. Soc., 37, 528-529.

Lee, J. T., 1971: Aerial survey of tornado-producing thunderstorms. Preprint of Seventh Conf. on Severe Local Storms, AMS, Kansas City, Missouri, 49-53.

McKowan, P. O., 1975: Data processing plan for Synchronous Meteorological and Geostationary Operational Environmental Satellites (SMS/GOES). Goddard Space Flight Center X-565-75-275, Greenbelt, Maryland, 276 p.

Miller, R. C., 1972: Notes on analysis and severe-storm forecasting procedures of the Air Force Global Weather Central. Air Weather Service Tech. Rept. 200, 190 p.

Negri, A. J., 1977: Satellite observations of onset and growth of severe local storms. Atmospheric Science Paper No. 278, Colorado State University, Fort Collins, Colorado, 89 p.

Pearl, E. W., W. E. Shenk and W. Skillman, 1975: Cloud top parameters-a hail indicator. Preprint of Ninth Conf. on Severe Local Storms, AMS, Norman, Oklahoma, 464-467.

Pitts, D. E., W. K. Reeser, and M. A. Mendlowitz, 1975: Equivalent blackbody temperature of the top of a severe storm. J. Appl. Meteor., 14, 609-618.

Purdom, J. F. W., 1971: Satellite imagery and severe weather warnings. Preprint of Seventh Conf. on Severe Local Storms, AMS, Kansas City, Missouri, 120-127.

Reynolds, D. W., M. L. Brown, E. A. Smith, and T. H. Vonder Haar, 1978: Cloud type separation by spectral differencing of image pairs. Submitted as a Note to Mon. Wea. Rev., 6 p.

Saunders, P. M. and F. C. Ronne, 1962: A comparison between the height of cumulus clouds and the height of radar echoes received from them. J. Appl. Meteor., 1, 296-302.

Sellers, W. D., 1965: Physical Climatology. The University of Chicago Press, Chicago and London, 272 p.

Serebreny, S. M., E. J. Wiegman, R. G. Hadfield, and W. E. Evans, 1970: Electronic system for utilization of satellite cloud pictures. Bull. Amer. Meteor. Soc., 51, 848-855.

Shenk, W. E., 1974: Cloud top height variability of strong convective cells. J. Appl Meteor., 13, 917-922.

Sikdar, D. N., V. E. Suomi, and C. E. Anderson, 1970: Convective transport of mass and energy in severe storms over the United States-an estimate from a geostationary altitude. Tellus, 22, 521-532.

Smith, E. A. and D. R. Phillips, 1972: Automated cloud tracking using precisely aligned digital ATS pictures. IEEE Transactions on Computers, C-21, 715-519.

Speed, D. K., 1965: General application of meteorological radar sets. Air Weather Service Tech. Rept. 184, 126 p.

Umenhofer, Thomas A., 1976: Overshooting top behavior of three tornado-producing thunderstorms. Preprint of Ninth Conf. on Severe Local Storms, Norman, Oklahoma, 96-99.

APPENDIX A

SEVERE STORM REPORTS FOR 5 MAY 1977

Severe weather reports for 5 May 1977 were obtained from the logs of the National Severe Storms Forecast Center in Kansas City, Missouri. Tables A-1 and A-3 contain a listing of reports applicable to this study. A summary of the severe weather occurrences may be found in the publication Storm Data.

Table A-1

Severe Storm Reports
(Texas - Oklahoma)

Time (GMT)	Event	Location
1715	Hail 4.4 cm (1.75 in)	Pecos, TX
1740	Tornado	37 km N Orla, TX
1815	Tornado	33 km S Lubbock, TX
1855	Tornado	12 km W O'Donnell, TX
1910	Funnel	Jal, NM
1930	Hail 4.4 cm (1.75 in)	Crosbyton, TX
1945	Funnel	13 km W Crowell, TX
2001	Hail 1. 9 cm (.75 in)	Midland, TX
2010	Hail 4.4 cm (1.75 in)	19 km E Crosbyton, TX
2026	Tornado	Hollis, Ok
2026	Tornado	El Dorado, OK
2050	Tornado	10 km SE Midland, TX
2050	Hail 7.0 cm (2.75 in)	Grassland, TX
2055	Funnel	6 km SW Willow, OK
2101	Funnel	34 km ENE Midland, TX
2240	Tornado	10 km W Rotan, TX
2245	Hail 4.4 cm (1.75 in)	2 km W Dickens, TX
2245	Tornado	2 km W Dickens, TX
2250	Funnel	7 km W Roby, TX
2300	Tornado	22 km W Aspermont, TX
2305	Wind Gust 34 ms^{-1} (67 kt)	Enid, OK
2350	Wind Gust 26 ms^{-1} (50 kt)	Dyess, AFB, TX

Table A-2

Severe Storm Reports
(Topeka - Kansas City)

Time (GMT)	Event	Location
2220	Hail 4.4 cm (1.75 in)	Topeka, KS
2327	Funnel	Topeka, KS
2320	Tornado	4 km SW Weston, MO
2345	Tornado	Topeka, KS
0005	Hail 2.5 cm (1.0 in)	11 km N Anthony, KS

Table A-3

Severe Storm Reports
(Missouri - Illinois)

Time (GMT)	Event	Location
2227	Hail 2.5 cm (1.0 in)	Knoxville, IL
2245	Tornado	Middletown, IA
2254	Funnel	Warsaw, IL
2300	Hail 4.4 cm (1.75 in)	Wentzville, MO
2320	Hail 4.4 cm (1.75 in)	Brimfield, IL
2343	Funnel	6 km S Bradford, IL
0003	Hail 3.8 cm (1.5 in)	Peoria, IL
0020	Hail 1.9 cm (.75 in)	7 km S Spring Bay, IL
0035	Hail 7.0 cm (2.75 in)	Philadelphia, IL

APPENDIX B

ALL DIGITAL VIDEO IMAGING SYSTEM FOR ATMOSPHERIC RESEARCH

The All Digital Video Imaging System for Atmospheric Research (ADVISAR) is a sophisticated combination of hardware and software which allows the user to interact quantitatively with a data set. The system is particularly well suited to the display and analysis of the large volume of information associated with satellite and similar digital data sets.

The main hardware components are illustrated schematically in Figure B-1 and pictorially in Figure B-2. The major component of the ADVISAR is the solid-state digital video refresh memory. It is possible to store up to eight digital images of 512 rows by 512 columns in the memory and selectively display any combination of the images on the video outputs. The video outputs include a color television monitor, two black and white monitors, and a video cassette recorder. The user interacts with the displayed data through an electronic cursor. The cursor is controlled by two joysticks which determine size and position or by system software which allows the cursor to be displayed in a variety of configurations and colors. The ADVISAR utilizes a Hewlett Packard 2100-A computer for system control. The user accesses the computer through one of two terminals; a cathode ray tube (CRT) display or a hardcopy terminal. Data may be entered into the system in two ways. The system includes 7-track and 9-track drives for reading digital tapes or writing stored images to tape. Additionally, the ADVISAR can digitize photographic images by using a vidicon camera to

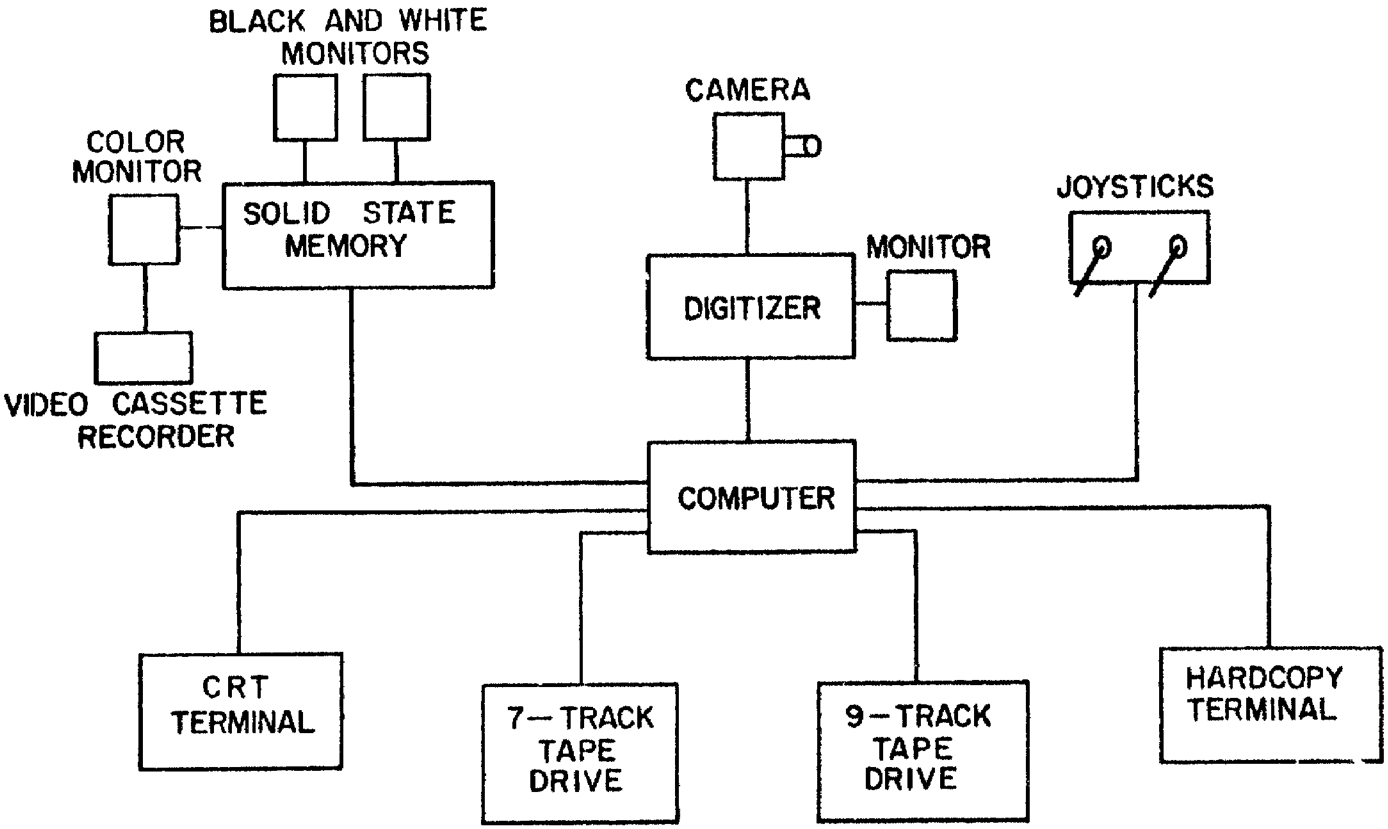

Figure B-1 Schematic diagram of ADVISAR showing major components.

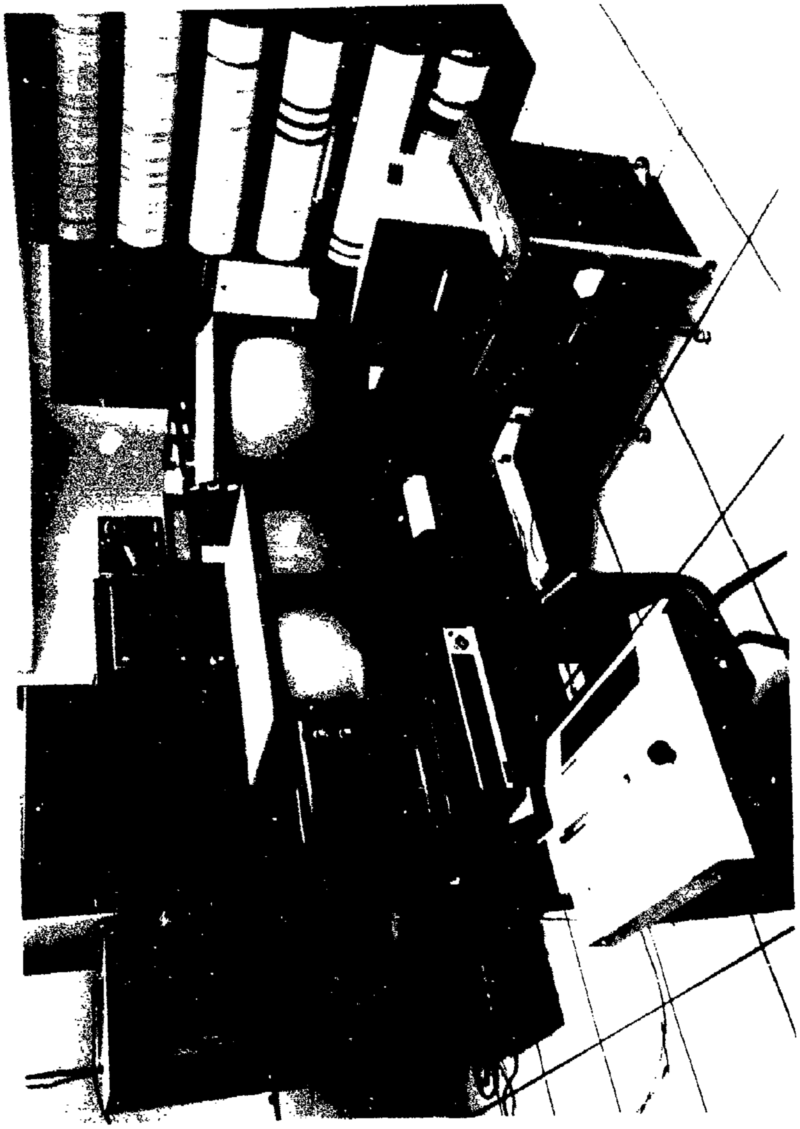

Figure B-2 The All Digital Video Imaging System for Atmospheric Research (ADVISAR).

create a video image. The image is then digitized into a 512 row by 480 column array which can be stored on memory or written to digital tape.

A wide variety of software is available for data manipulation. Computer programs are currently available to compute histograms of data values, difference and average two images pixel-for-pixel, color enhance images, loop through a time sequence of images to show cloud motion and to perform numerous other functions. A versatile graphics package is also available. All software is easily accessible to the user with a minimum of instruction.

The ADVISAR is in the process of being upgraded through the addition of a larger and more powerful computer. An SMS/GOES ground station is also being added giving real-time data access as well as greater availability of satellite data sets for research. A more detailed description of the ADVISAR is given by Brown (1978).

APPENDIX C

CATALOG OF SATELLITE DATA FOR 5 MAY 1977

Satellite data from the 5 May 1977 Rapid Scan Research Day was registered by landmark matching. A catalog of the visible and IR data is presented in Tables C-1 and C-2. The relative line and element shifts are those necessary to match landmarks from each image to the 1730 GMT image. Any two images displayed using the indicated shifts should be precisely aligned geographically.

Table C-1

Catalog of Visible Data 5 May 1977

Tape No.	File	Time (GMT)	Relative Shift		Comments
			Element	Line	
F9731	2	1730	0	0	Grid
	4	1739	0	154	Grid
	6	1742	0	80	Bad File
	8	1745	0	163	
	10	1748	0	70	
	12	1751	0	164	
F9732	2	1754	1	85	
	4	1800	2	-2	Grid
	6	1809	2	184	Grid
	8	1812	2	129	
	10	1815	3	89	
	12	1818	3	18	
F9733	2	1821	4	107	
	4	1824	4	36	
	6	1830	4	-3	Grid
	8	1839	4	-90	Grid
	10	1842	4	-169	
	11	1845	4	-80	
F9734	2	1848	4	-152	
	4	1851	4	-104	
	6	1854	4	-152	
	7	1900	4	-4	Grid
	10	1909	4	+151	Grid
	12	1912	4	+128	

Table C-1

Tape No.	File	Time (GMT)	Relative Shift		Comments
			Element	Line	
F9735	2	1915	6	240	
	4	1918	6	176	
	6	1921	6	265	
	8	1924	6	179	
	10	1930	6	-4	Grid
	12	1939	6	32	Grid
F9736	2	1942	6	-48	
	4	1945	6	58	
	6	1948	6	-6	
	8	1951	6	83	
	10	1954	6	12	
	12	2000	6	-2	Grid
F9737	2	2009	8	152	Grid
	4	2012	8	96	
	6	2015	8	2	
	8	2018	8	-69	
	10	2021	8	29	
	12	2024	8	-35	
F9738	2	2030	8	-9	Grid
	4	2039	8	155	Grid
	7	2042	8	99	
	9	2045	8	228	
	11	2048	8	149	
	13	2051	8	158	

Table C-1

Tape No.	File	Time (GMT)	Relative Shift Element	Relative Shift Line	Comments
F9739	2	2054	10	120	
	3	2100	9	-7	Grid
	5	2109	10	451	Grid
	7	2112	10	349	
	10	2115	10	355	Bad File
	12	2118	10	327	
F9740	2	2121	10	353	
	4	2124	10	416	
	6	2130	11	-3	Grid
	8	2139	10	231	Grid
	10	2142	10	160	
	12	2145	10	173	
F9741	2	2148	10	178	
	4	2151	10	219	
	6	2154	10	140	
	8	2200	10	-2	Grid
	10	2209	10	296	Grid
	12	2212	10	-87	
F9742	2	2215	10	283	
	4	2218	10	196	
	6	2221	10	261	
	8	2224	10	150	
	11	2230	10	-9	Grid
	13	2239	10	267	Grid

Table C-1

Tape No.	File	Time (GMT)	Relative Shift		Comments
			Element	Line	
F9743	2	2242	10	189	
	4	2245	10	253	
	6	2248	10	182	
	8	2251	10	240	
	10	2254	10	160	
	12	2300	10	-6	Grid
F9744	2	2309	10	269	Grid
	4	2312	10	198	
	6	2315	10	246	
	8	2318	10	176	
	10	2321	10	216	
	12	2324	10	137	
F9745	2	2330	+10	-5	Grid
	4	2339	-120	253	Grid Shifted
	6	2342	-120	190	
	8	2345	-120	264	
	10	2348	-120	176	
	12	2351	-120	226	
F9746	2	2354	-120	152	
	4	0000	-120	-5	Grid Shifted
	6	0009	-120	294	Grid Shifted
	8	0012	-120	216	
	10	0015	-120	248	
	12	0018	-120	176	

Table C-1

Tape No.	File	Time (GMT)	Relative Shift Element	Relative Shift Line	Comments
F9747	2	0021	-120	240	
	4	0024	-120	160	
	6	0030	+10	-4	Grid
	8	0039			Too Dark
	10	0042			Too Dark
	12	0045			Too Dark
F9748	2	0048			Too Dark
	4	0051			Too Dark

Table C-2

Catalog of Infrared Data 5 May 1977

Tape No.	File	Time (GMT)	Relative Shifts Element	Relative Shifts Line	Comments
F9060	1	1730	0	0	Grid
	2	1739	0	18	Grid
	3	1742	0	9	
	4	1745	0	20	
	5	1748	0	8	
	6	1751	0	19	
	7	1754	0	9	
	8	1800	0	0	Grid
	9	1809	0	22	Grid
	10	1812	0	16	
	11	1815	0	10	
	12	1818	0	2	
	13	1821	0	13	
	14	1824	0	4	
	15	1830	0	0	Grid
	16	1839	0	-11	Grid
	17	1842	0	-21	
	18	1848	0	-17	
	19	1851	0	-13	
	20	1854	0	-19	
	22	1845	0	-10	
	23	1900	0	0	Grid
F9075	20	1909	0	20	Grid
	21	1912	0	16	
	22	1915	0	30	
	23	1918	0	22	
	24	1921	0	33	

Table C-2

Tape No.	File	Time (GMT)	Relative Shifts Element	Relative Shifts Line	Comments
F9066	1	1930	0	0	Grid
	2	1939	0	3	Grid
	3	1942	0	-6	
	4	1945	0	7	
	5	1948	0	-2	
	6	1951	0	10	
	7	1954	0	2	Short File
	9	2000	0	0	Grid
	10	2009	0	19	Grid, Short File
	11	2012	0	14	
	12	2015	0	2	
	13	2018	0	-8	
	14	2021	0	4	
	15	2024	0	-4	
	17	2009	0	19	Grid
	18	2039	0	20	Grid
	19	2042	0	13	
	20	2045	0	29	
	21	2048	0	19	
	22	2051	0	20	
	23	2054	0	15	
	25	2100	0	0	Grid
	26	2109	0	57	Grid
	27	2112	0	44	
	28	2115	0	45	
	29	2118	0	41	
	30	2121	0	45	
	31	2124	0	53	
	32	2130	0	0	Grid
	34	2139	0	29	Grid
	35	'142	0	20	

Table C-2

Tape No.	File	Time (GMT)	Relative Shifts Element	Relative Shifts Line	Comments
F9066/	36/2	2145	0	24	Lines Missing
F9075	37/3	2148	0	23	
	38/4	2151	0	28	
F9075	5	2154	0	18	
	6	2200	0	0	Grid
	7	2209	0	37	Grid
	8	2212	0	-10	
	9	2215	0	36	
	10	2218	0	25	
	11	2221	0	33	
	12	2224	0	19	
	13	2230	0	-1	Grid
F9075/	14/1	2239	0	34	Grid
F9061	15/2	2242	0	24	
	16/3	2245	0	32	Lines Missing
	17/4	2248	0	23	
	18/5	2251	0	30	
	19/6	2254	0	20	
F9061	7	2300	0	0	Grid
	8	2309	0	34	Grid
	9	2312	0	25	
	10	2315	0	31	
	11	2318	0	23	
	12	2321	0	28	
	13	2324	0	18	
	14	2330	0	0	Grid
	15	2339	-30	34	Grid Shifted

Table C-2

Tape No.	File	Time (GMT)	Relative Shifts Element	Line	Comments
F9061	16	2342	-30	24	
	18	2345	-30	34	
	19	2348	-30	23	
	20	2351	-30	29	
	21	2354	-30	20	
	22	0000	-30	0	Grid Shifted
	23	0009	-30	37	Grid Shifted
	24	0012	-30	27	
	25	0015	-30	31	
	26	0018	-30	23	
	27	0021	-30	31	
F9075	1	0024	-30	-2	